

Shape Optimization of Compliant Pressure Actuated Cellular Structures

Markus Pagitz* and Remco I. Leine

Institute for Nonlinear Mechanics, University of Stuttgart, Stuttgart, 70569, Germany

Abstract

Previous work introduced a novel concept for pressure actuated cellular structures that can change their shape between any two given one-dimensional C^1 continuous functions. However, the underlying computational framework is limited to two cell rows and central cell corner hinges. This article extends these results by taking into account an arbitrary number of cell rows, hinge eccentricities and rotational as well as axial cell side springs. This allows the design of compliant pressure actuated cellular structures that can change their shape between any given set of one-dimensional C^1 continuous functions. Furthermore, we introduce a potential based optimization approach that reduces the previously required number of iterations by an order of magnitude. Finally, it is shown how the optimization can be tightly coupled to the geometry of a cellular structure. Several examples are presented that demonstrate the performance of the proposed framework.

Keywords *adaptive - biomimetic - cellular - compliant - morphing - structure*

*markus.pagitz@inm.uni-stuttgart.de

Notation

SUPERSCRIPTS

| | |
|---|---------------------------------------|
| \star | reduced variable |
| 0 | reference configuration OR derivative |
| P, S, T | reference to pentagon, side, triangle |
| $\beta, \mathbf{u}, \mathbf{v}, \mathbf{w}, \mathbf{x}$ | derivative |

SUBSCRIPTS

| | |
|-----------|--|
| aug | augmented |
| max | maximum |
| min | minimum |
| opt | optimization |
| ult | ultimate |
| vir | virtual |
| 0 | reference configuration |
| α | state variables of cells with central cell corner hinges |
| κ | state variables for hinge eccentricities |
| x, y | cartesian vector components |
| $-, +$ | lower, upper cell side |
| a, b, c | cell side reference |
| e, h | rotational, axial springs |
| o | obstacle |
| p | pressure |
| q | pressure set |

VARIABLES

| | |
|--------------------------------------|---|
| α, β | state angle of cellular structure |
| Δ | difference |
| δ | Kronecker delta |
| η | weighting factor |
| θ | internal angle of pentagonal, triangular cell |
| κ | state angle for hinge eccentricities |
| λ | factor, Lagrange multiplier |
| ξ | base side coordinate |
| Π | energy |
| ρ | distinction of cases |
| φ | bending angle of cell side |
| ω | geometric parameter |
| n^α, n^κ | number of state variables |
| n^C, n^L, n^P | number of cells, cell levels, base pentagons |
| $n^v, n^w, n^{x\kappa}$ | number of sides, eccentricities, rotational springs |
| A | cross sectional area |
| \mathbf{A}, \mathbf{B} | matrices for elimination of axial degrees of freedom |
| \mathbf{C} | constraint matrix |
| a, b, c | cell side |
| d | hinge eccentricity |
| e | rotational spring |
| \mathbf{G}, \mathbf{g} | gradient matrix, vector |
| \mathbf{h} | axial stiffness |
| i, j | integer |
| L | length |
| \mathbf{m} | mixed variables |
| p | pressure |
| r, \mathbf{r} | radius, residual vector |
| \mathbf{T} | transformation matrix |
| $\mathbf{u}, \mathbf{v}, \mathbf{w}$ | state variables, side lengths, hinge eccentricities of cellular structure |
| X | placeholder |
| \mathbf{x} | springs of cellular structure |
| y, z | internal length of pentagonal cell |

1 Introduction

There exists a wide range of technologies that would immensely benefit from robust, strong, lightweight and energy efficient compliant structures that can change their shape between any set of one-dimensional C^1 continuous functions. For example, currently used aircraft slats are relatively heavy and the gaps between wings and slats increase noise levels particularly during take off and landing. A comparison of existing actuation principles [5] shows that pressure based actuators have the greatest potential to create such structures (Figure 1). Hence it is not surprising that the pressure driven nastic movement of plants attracted a lot of attention during the last decade. The results of a considerable research effort in this field that was backed up by the Defense Advanced Research Agency, National Science Foundation and the United States Army can be found in the book edited by Wereley and Sater [19]. A comprehensive understanding of the nastic movement of plants requires various disciplines that range from biology and chemistry to material science and structural engineering. The focus of this article is on the structural engineering side. Therefore, no attention is given to the functionality of sub-cellular hydration motors [16] or plant cell materials [7]. Instead it is assumed that cellular structures are made from common engineering materials and that cell pressures are provided by an external source such as a compressor. Furthermore, only prismatic cells are considered. Hence, the problem reduces to the understanding of two-dimensional cell geometries and their interactions.

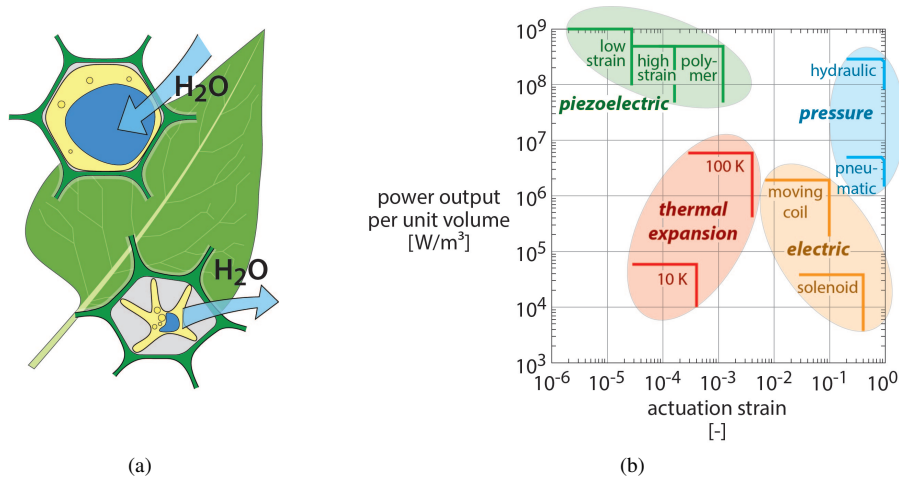


Figure 1: (a) Osmotic hydration motors are used to vary cell pressures and thus to alter cell geometries. (b) Power output per unit volume versus strain of various actuation principles (data from Huber et al [5]).

An overview of publications that investigate prismatic pressure actuated cellular structures is subsequently given. A concept that is based on plane symmetry groups was patented by Dittrich [1]. Dittrich combined convex and concave cells to create actuators that can replace double acting cylinders. A similar approach that uses pressurized and void cells was investigated by Luo and Tong [17]. Although not directly related to adaptive structures, Khire et al [8] studied inflatable structures that are made from a large number of uniformly pressurized hexagonal cells. Vos and Barret [18] subsequently patented a similar concept. Further work that investigates pressurized honeycombs can be found in [3, 4, 6]. Numerical tools for the simulation and optimization of two-dimensional cellular structures were, among others, published by Lv et al [9, 10]. A novel concept for pressure actuated cellular structures that are made from separately pressurized rows of individually tailored prismatic cells (Figure 2) was patented by Pagitz et al [11, 12]. It was shown [15] that these structures can be made from arbitrary materials that range from elastomers to steel. Furthermore it was shown [13] that cytoskeletons can be used within each cell to reduce, increase the structural weight, stiffness. However, the underlying numerical framework is limited to cellular structures with two cell rows and central cell corner hinges (Figure 3a). The aim of this article is to extend previous work by taking into account an arbitrary number of cell rows, hinge eccentricities and rotational as well as axial springs (Figure 3b). This allows the design of compliant pressure actuated cellular structures that can change their shape between any given set of one-dimensional

C^1 continuous functions. Furthermore we introduce a potential based optimization approach that reduces the required number of iterations by an order of magnitude. Finally it is shown how the proposed framework can be tightly coupled to the geometry of a cellular structure.

The outline of this article is as follows: Section 2 introduces state and optimization variables as well as geometric and energy terms of a single pentagonal cell with central cell corner hinges. Similar expressions for a triangular cell are derived in Section 3. Cell side properties due to non-zero hinge eccentricities and rotational springs are given in Section 4. State and optimization variables of a cellular structures with eccentric cell corner hinges and rotational springs are presented in Section 5. It is shown that the proposed framework reduces to the numerical model published in [11] if hinge eccentricities and rotational springs are small. The computation of equilibrium and optimal reference configurations as well as the optimization of cell side lengths for given target shapes is outlined. Previously published optimization approach is enhanced with a potential based approach that reduces the number of iterations by an order of magnitude. Section 6 introduces additional state variables for the consideration of axial strains and outlines the computation of corresponding equilibrium configurations and optimal cell side lengths. Section 7 presents several examples that demonstrate the performance of the numerical method. Section 8 shows how the proposed framework can be tightly coupled to the geometry of a cellular structure. Section 9 concludes the article.

2 Pentagonal Cell

2.1 Geometric Properties

Pressure actuated cellular structures consist of pentagonal and hexagonal cells where the latter can be split into a pentagonal and triangular part. Cell side-, internal lengths and state-, internal angles of a single pentagonal cell are shown in Figure 4. It can be seen that hinge eccentricities as well as rotational and axial springs are not considered. This is possible since the corresponding effects can be later added without loss of accuracy. State variables \mathbf{u}_α^P and cell sides \mathbf{v}^P are

$$\mathbf{u}_\alpha^P = \begin{bmatrix} \alpha_1^P & \alpha_2^P & a^P \end{bmatrix}^T \quad \text{and} \quad \mathbf{v}^P = \begin{bmatrix} b_1^P & b_2^P & c_1^P & c_2^P \end{bmatrix}^T. \quad (1)$$

Note that a superscript ‘‘P’’ is used for state and optimization variables that define the geometry of a pentagonal cell. Furthermore, it is used for internal variables that could be confused with subsequently derived variables. The length of line y that divides the pentagon into a triangular and quadrilateral part is

$$y = \sqrt{y_x^2 + y_y^2} = \sqrt{(a^P + \sin(\alpha_2^P)b_2^P - \sin(\alpha_1^P)b_1^P)^2 + (\cos(\alpha_2^P)b_2^P - \cos(\alpha_1^P)b_1^P)^2} \quad (2)$$

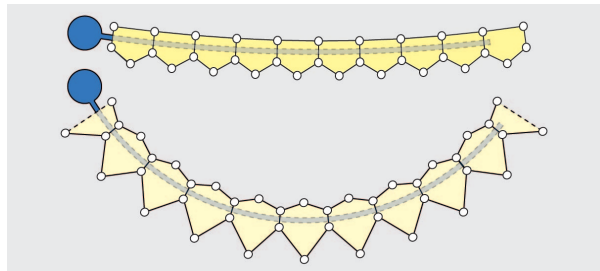
and its first-order derivatives with respect to state variables \mathbf{u}_α^P and cell sides \mathbf{v}^P are

$$\frac{\partial y}{\partial \mathbf{u}_\alpha^P} = \frac{1}{y} \begin{bmatrix} (\sin(\alpha_1^P - \alpha_2^P)b_2^P - a^P \cos(\alpha_1^P))b_1^P \\ -(\sin(\alpha_1^P - \alpha_2^P)b_1^P - a^P \cos(\alpha_2^P))b_2^P \\ y_x \end{bmatrix} \quad \text{and} \quad \frac{\partial y}{\partial \mathbf{v}^P} = \frac{1}{y} \begin{bmatrix} -\sin(\alpha_1^P)a^P - \cos(\alpha_1^P - \alpha_2^P)b_2^P + b_1^P \\ \sin(\alpha_2^P)a^P - \cos(\alpha_1^P - \alpha_2^P)b_1^P + b_2^P \\ 0 \\ 0 \end{bmatrix}. \quad (3)$$

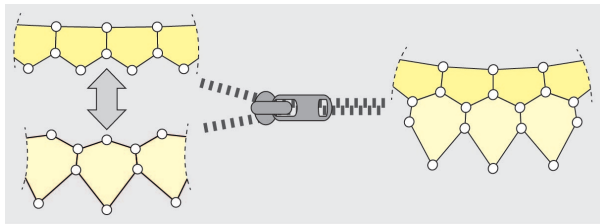
The altitude z of a pentagonal cell is

$$z = \sqrt{c_1^{P2} - \frac{1}{4y^2}(y^2 + c_1^{P2} - c_2^{P2})^2} \quad (4)$$

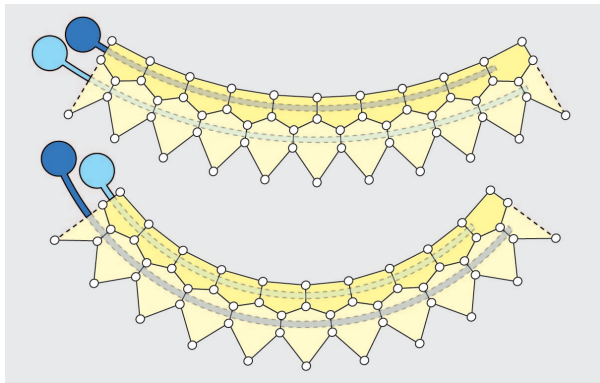
so that its first-order derivatives with respect to base side y and cell sides $\mathbf{c}^P = \begin{bmatrix} c_1^P & c_2^P \end{bmatrix}^T$ are



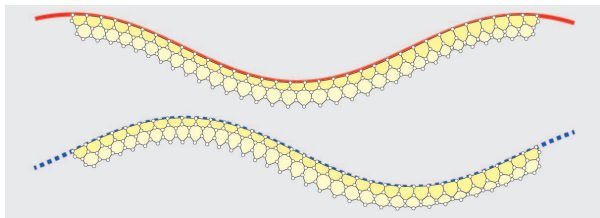
(a)



(b)



(c)



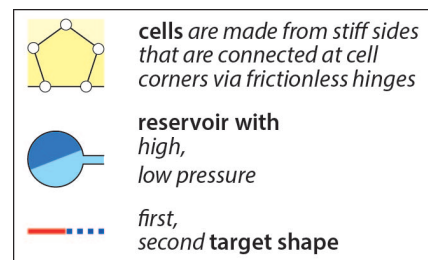
(d)

Figure 2: (a) A cantilever that is assembled from a number of identical prismatic cells with pentagonal or hexagonal cross sections deforms after pressurization into a circular arc. Corresponding radius is independent of cell pressures and solely a function of cell side lengths.

(b) Two cantilevers that are made from either pentagonal or hexagonal cells can be connected if opposite cell sides are of equal length.

(c) Equilibrium shape of a structure that is made from two connected cell rows can be altered by changing the pressure ratio between cell rows.

(d) Individually tailoring the cell side lengths allows the design of cellular structures that can change their shape between any two given one-dimensional C^1 continuous functions.



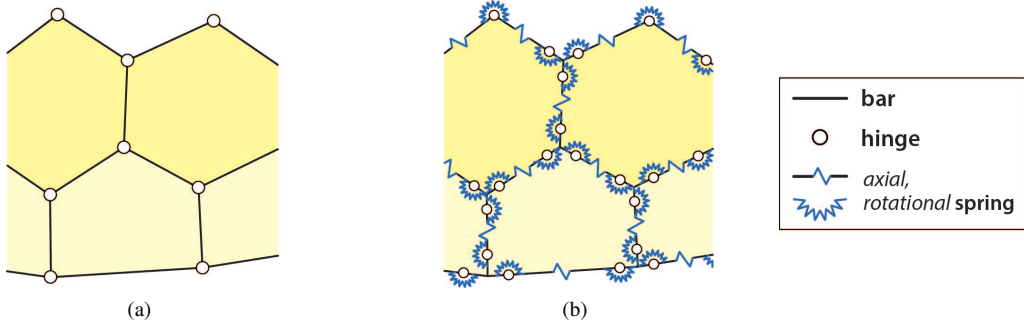


Figure 3: Cellular structure with (a) central and (b) eccentric cell corner hinges and rotational, axial springs.

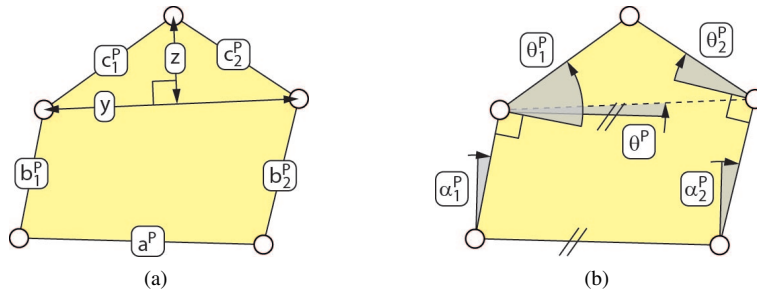


Figure 4: (a) Cell side-, internal lengths and (b) state-, internal angles of a pentagonal cell.

$$\frac{\partial z}{\partial y} = \frac{1}{4y^3z} \left((c_1^{P2} - c_2^{P2})^2 - y^4 \right) \quad \text{and} \quad \frac{\partial z}{\partial \mathbf{c}^P} = \frac{1}{2y^2z} \begin{bmatrix} c_1^P (y^2 - c_1^{P2} + c_2^{P2}) & c_2^P (y^2 + c_1^{P2} - c_2^{P2}) \end{bmatrix}^\top. \quad (5)$$

Hence, first-order derivatives with respect to pentagonal state variables \mathbf{u}_α^P and cell sides \mathbf{v}^P are

$$\frac{\partial z}{\partial \mathbf{u}_\alpha^P} = \frac{\partial z}{\partial y} \frac{\partial y}{\partial \mathbf{u}_\alpha^P} \quad \text{and} \quad \frac{\partial z}{\partial \mathbf{v}^P} = \frac{\partial z}{\partial y} \frac{\partial y}{\partial \mathbf{v}^P} + \frac{\partial z}{\partial \mathbf{c}^P} \frac{\partial \mathbf{c}^P}{\partial \mathbf{v}^P} \quad (6)$$

where $\partial \mathbf{c}^P / \partial \mathbf{v}^P$ can be considered to be an element freedom table. The inclination θ^P between base side a^P and y is

$$\theta^P = \arcsin \left(\frac{y_y}{y} \right) \quad (7)$$

so that its first-order derivatives with respect to state variables \mathbf{u}_α^P and cell sides \mathbf{v}^P are

$$\frac{\partial \theta^P}{\partial \mathbf{u}_\alpha^P} = \frac{1}{y_x} \left(\frac{\partial y_y}{\partial \mathbf{u}_\alpha^P} - \frac{y_y}{y} \frac{\partial y}{\partial \mathbf{u}_\alpha^P} \right) \quad \text{and} \quad \frac{\partial \theta^P}{\partial \mathbf{v}^P} = \frac{1}{y_x} \left(\frac{\partial y_y}{\partial \mathbf{v}^P} - \frac{y_y}{y} \frac{\partial y}{\partial \mathbf{v}^P} \right). \quad (8)$$

The internal angle θ_1^P of a pentagonal cell is

$$\theta_1^P = \begin{cases} \alpha_1^P + \theta^P + \arcsin \left(\frac{z}{c_1^P} \right), & c_2^{P2} \leq y^2 + c_1^{P2} \\ \alpha_1^P + \theta^P - \arcsin \left(\frac{z}{c_1^P} \right) + \pi, & c_2^{P2} > y^2 + c_1^{P2} \end{cases} \quad \text{and} \quad \rho_1 = \begin{cases} +1, & c_2^{P2} \leq y^2 + c_1^{P2} \\ -1, & c_2^{P2} > y^2 + c_1^{P2} \end{cases} \quad (9)$$

and its first-order derivatives with respect to state variables \mathbf{u}_α^P and cell sides \mathbf{v}^P are

$$\begin{aligned} \frac{\partial \theta_1^P}{\partial \mathbf{u}_\alpha^P} &= + \frac{\partial \theta^P}{\partial \mathbf{u}_\alpha^P} + \frac{\rho_1}{\sqrt{c_1^{P2} - z^2}} \frac{\partial z}{\partial \mathbf{u}_\alpha^P} + \begin{bmatrix} 1 & 0 & 0 \end{bmatrix}^\top \\ \frac{\partial \theta_1^P}{\partial \mathbf{v}^P} &= + \frac{\partial \theta^P}{\partial \mathbf{v}^P} + \frac{\rho_1}{\sqrt{c_1^{P2} - z^2}} \left(\frac{\partial z}{\partial \mathbf{v}^P} - \frac{z}{c_1^P} \begin{bmatrix} 0 & 0 & 1 & 0 \end{bmatrix}^\top \right). \end{aligned} \quad (10)$$

Note that expressions for the internal angle θ_2^P are derived in a similar manner. Furthermore, previous equations could be written without a distinction of cases. However, this would result in lengthier expressions.

2.2 Pressure Potential

The pressure potential of a pentagonal cell with central cell corner hinges and an internal pressure p is

$$\Pi^P = -pA^P = -\frac{p}{2} \left((\cos(\alpha_1^P) b_1^P + \cos(\alpha_2^P) b_2^P) a^P + \sin(\alpha_2^P - \alpha_1^P) b_1^P b_2^P + yz \right) \quad (11)$$

where A^P is the cross-sectional area of the pentagon. The first-order derivatives with respect to state variables \mathbf{u}_α^P and cell sides \mathbf{v}^P are

$$\begin{aligned}\mathbf{\Pi}^{P, \mathbf{u}_\alpha} &= -\frac{p}{2} \left(\begin{bmatrix} -(\sin(\alpha_1^P) a^P + \cos(\alpha_2^P - \alpha_1^P) b_2^P) b_1^P \\ -(\sin(\alpha_2^P) a^P - \cos(\alpha_2^P - \alpha_1^P) b_1^P) b_2^P \\ \cos(\alpha_1^P) b_1^P + \cos(\alpha_2^P) b_2^P \end{bmatrix} + z \frac{\partial y}{\partial \mathbf{u}_\alpha^P} + y \frac{\partial z}{\partial \mathbf{u}_\alpha^P} \right) \\ \mathbf{\Pi}^{P, \mathbf{v}} &= -\frac{p}{2} \left(\begin{bmatrix} \cos(\alpha_1^P) a^P + \sin(\alpha_2^P - \alpha_1^P) b_2^P \\ \cos(\alpha_2^P) a^P + \sin(\alpha_2^P - \alpha_1^P) b_1^P \\ 0 \\ 0 \end{bmatrix} + z \frac{\partial y}{\partial \mathbf{v}^P} + y \frac{\partial z}{\partial \mathbf{v}^P} \right).\end{aligned}\quad (12)$$

Corresponding second-order derivatives are denoted as $\mathbf{\Pi}^{P, \mathbf{u}_\alpha \mathbf{u}_\alpha}$, $\mathbf{\Pi}^{P, \mathbf{u}_\alpha \mathbf{v}}$ and $\mathbf{\Pi}^{P, \mathbf{v} \mathbf{v}}$.

3 Triangular Cells

3.1 Geometric Properties

A triangular cell is defined by two neighbouring pentagonal cells. It constitutes, together with a pentagonal cell in the upper row a hexagonal cell. Like previously we consider only central cell corner hinges. Cell side-, base lengths and state-, internal angles of a triangular cell are shown in Figure 5. State variables \mathbf{u}_α^T and cell sides \mathbf{v}^T are

$$\mathbf{u}_\alpha^T = \begin{bmatrix} \alpha_1^T & \alpha_2^T & \alpha_3^T & \alpha_4^T & a_1^T & a_2^T \end{bmatrix}^T \quad \text{and} \quad \mathbf{v}^T = \begin{bmatrix} b_1^T & b_2^T & b_3^T & c_1^T & c_2^T & c_3^T & c_4^T \end{bmatrix}^T \quad (13)$$

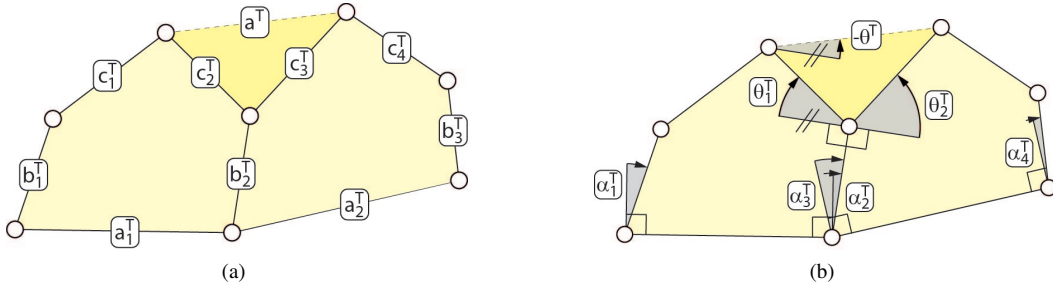


Figure 5: (a) Cell side-, base lengths and (b) state-, internal angles of a triangular cell.

where superscript “T” is used for state and optimization variables as well as internal variables of a triangular cell. The abstract side a^T that is the base side of the adjacent pentagonal cell is

$$a^T = \sqrt{c_2^{T^2} + c_3^{T^2} + 2c_2^T c_3^T \cos(\theta_1^T + \theta_2^T)}. \quad (14)$$

First-order derivatives with respect to state variables \mathbf{u}_α^T and cell sides \mathbf{v}^T are

$$\begin{aligned}\frac{\partial a^T}{\partial \mathbf{u}_\alpha^T} &= -\frac{1}{a^T} c_2^T c_3^T \sin(\theta_1^T + \theta_2^T) \frac{\partial(\theta_1^T + \theta_2^T)}{\partial \mathbf{u}_\alpha^T} \\ \frac{\partial a^T}{\partial \mathbf{v}^T} &= -\frac{1}{a^T} \left(c_2^T c_3^T \sin(\theta_1^T + \theta_2^T) \frac{\partial(\theta_1^T + \theta_2^T)}{\partial \mathbf{v}^T} - \begin{bmatrix} 0 & 0 & 0 & 0 & c_2^T + c_3^T \cos(\theta_1^T + \theta_2^T) & c_3^T + c_2^T \cos(\theta_1^T + \theta_2^T) & 0 \end{bmatrix}^T \right).\end{aligned}\quad (15)$$

The internal angle θ^T of a triangular cell is

$$\theta^T = \theta_1^T - \arccos\left(\frac{a^{T^2} + c_2^{T^2} - c_3^{T^2}}{2a^T c_2^T}\right) \quad (16)$$

so that its first-order derivatives with respect to base side a^T and cell sides $\mathbf{c}^T = [c_1^T \ c_2^T \ c_3^T \ c_4^T]^T$ are

$$\frac{\partial \theta^T}{\partial a^T} = \frac{1}{a^T X} (a^{T^2} - c_2^{T^2} + c_3^{T^2}) \quad \text{and} \quad \frac{\partial \theta^T}{\partial \mathbf{c}^T} = -\frac{1}{c_2^T X} \begin{bmatrix} 0 & a^{T^2} - c_2^{T^2} - c_3^{T^2} & 2c_2^T c_3^T & 0 \end{bmatrix}^T \quad (17)$$

where

$$X = \sqrt{(2a^T c_2^T)^2 - (a^{T^2} + c_2^{T^2} - c_3^{T^2})^2}. \quad (18)$$

Hence, first-order derivatives with respect to state variables \mathbf{u}_α^T and cell sides \mathbf{v}^T are

$$\frac{\partial \theta^T}{\partial \mathbf{u}_\alpha^T} = \frac{\partial \theta_1^T}{\partial \mathbf{u}_\alpha^T} + \frac{\partial \theta^T}{\partial a^T} \frac{\partial a^T}{\partial \mathbf{u}_\alpha^T} \quad \text{and} \quad \frac{\partial \theta^T}{\partial \mathbf{v}^T} = \frac{\partial \theta_1^T}{\partial \mathbf{v}^T} + \frac{\partial \theta^T}{\partial a^T} \frac{\partial a^T}{\partial \mathbf{v}^T} + \frac{\partial \theta^T}{\partial \mathbf{c}^T} \frac{\partial \mathbf{c}^T}{\partial \mathbf{v}^T}. \quad (19)$$

3.2 Pressure Potential

The pressure potential of a triangular cell without hinge eccentricities is

$$\Pi^T = -\frac{p}{2} c_2^T c_3^T \sin(\theta_1^T + \theta_2^T) \quad (20)$$

and its first-order derivatives with respect to state variables \mathbf{u}_α^T and cell sides \mathbf{v}^T are

$$\begin{aligned} \Pi^{T, \mathbf{u}_\alpha} &= -\frac{p}{2} c_2^T c_3^T \cos(\theta_1^T + \theta_2^T) \frac{\partial(\theta_1^T + \theta_2^T)}{\partial \mathbf{u}_\alpha^T} \\ \Pi^{T, \mathbf{v}} &= -\frac{p}{2} \left(c_2^T c_3^T \cos(\theta_1^T + \theta_2^T) \frac{\partial(\theta_1^T + \theta_2^T)}{\partial \mathbf{v}^T} + \sin(\theta_1^T + \theta_2^T) \begin{bmatrix} 0 & 0 & 0 & 0 & c_3^T & c_2^T & 0 \end{bmatrix}^T \right). \end{aligned} \quad (21)$$

4 Cell Sides

4.1 Geometric Properties

The previously published numerical framework [11] assumes rigid cell sides that are connected at cell corners via frictionless hinges. This assumption is valid as long as cell sides are relatively thin. It is subsequently shown how the influence of rotational springs and hinge eccentricities at cell corners can be taken into account. We assume that undeformed cell sides are straight and that, although rigid body motions might be large, rotations at hinges are small. This assumption is valid since cell side rotations in compliant structures are limited by material properties. Hence it is possible to assume that cell side lengths are invariant to cell corner rotations. Nevertheless, a similar approach could be used for arbitrarily large rotations. However, this would increase the number of coupling terms and thus complicate the following derivations. Therefore, in order to increase readability, the consideration of axial strains

is separately outlined in Section 6. The required state and optimization variables as well as hinge eccentricities and rotational springs of a single cell side (Figure 6) are

$$\mathbf{u}_\kappa^S = \begin{bmatrix} \kappa_-^S & \kappa_+^S \end{bmatrix}^\top, \quad \nu^S = \begin{bmatrix} L^S \end{bmatrix}, \quad \mathbf{w}^S = \begin{bmatrix} d_-^S & d_+^S \end{bmatrix}^\top \quad \text{and} \quad \mathbf{x}_\kappa^S = \begin{bmatrix} e_-^S & e_+^S \end{bmatrix}^\top. \quad (22)$$

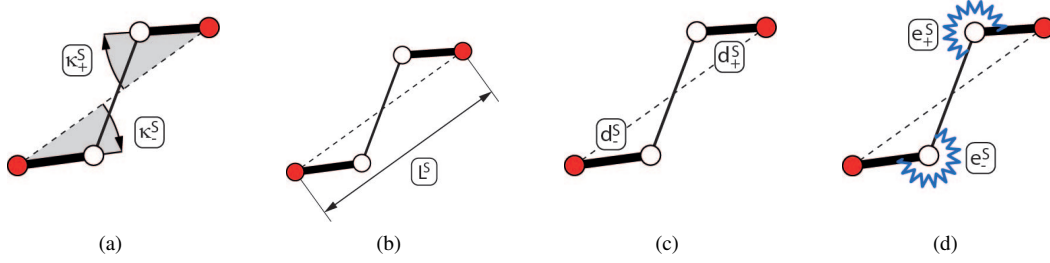


Figure 6: (a) State variables, (b) length, (c) hinge eccentricities and (d) springs of a single cell side.

The additional global state variables \mathbf{u}_κ for the hinge eccentricities at cell corners are expressed with respect to cell sides “b”. Hence it is possible to directly write down the state variables \mathbf{u}_κ^S of cell sides “b” as

$$\begin{bmatrix} \kappa_{b1-}^S & \kappa_{b1+}^S \end{bmatrix}^\top = \begin{bmatrix} \kappa_{1-}^S & \kappa_{1+}^S \end{bmatrix}^\top \quad \text{and} \quad \begin{bmatrix} \kappa_{b2-}^S & \kappa_{b2+}^S \end{bmatrix}^\top = \begin{bmatrix} \kappa_{2-}^S & \kappa_{2+}^S \end{bmatrix}^\top. \quad (23)$$

In contrast, state variables \mathbf{u}_κ^S of cell sides “a” and “c” are not only a function of global state variables \mathbf{u}_κ but also of local \mathbf{u}_α^P , global β^P pentagonal state variables as shown in Figure 7 so that

$$\begin{bmatrix} \kappa_{a1-}^S \\ \kappa_{a1+}^S \end{bmatrix} = \begin{bmatrix} \kappa_{1-}^S + \Delta\alpha_1^P \\ \kappa_{2-}^S + \Delta\alpha_2^P \end{bmatrix}, \quad \begin{bmatrix} \kappa_{c1-}^S \\ \kappa_{c1+}^S \end{bmatrix} = \begin{bmatrix} \kappa_{1-}^S - \Delta\alpha_1^P + \Delta\theta_1^P + \Delta\beta^P \\ \kappa_{3-}^S - \Delta\alpha_1^P + \Delta\theta_1^P + \Delta\beta^P \end{bmatrix} \quad \text{and} \quad \begin{bmatrix} \kappa_{c2-}^S \\ \kappa_{c2+}^S \end{bmatrix} = \begin{bmatrix} \kappa_{2+}^S - \Delta\alpha_2^P - \Delta\theta_2^P + \Delta\beta^P \\ \kappa_{3-}^S - \Delta\alpha_2^P - \Delta\theta_2^P + \Delta\beta^P \end{bmatrix}. \quad (24)$$

Note that, for example, $\Delta\alpha = \alpha - \alpha^0$ is the difference of α between the current and reference configuration. In other words, current state variables of cell sides depend on the reference configuration. Furthermore it should be noted that $\beta^P = 0$ for the outer cell row. Bending angles of a single cell side are

$$\varphi_-^S = \frac{1}{L^S - d_-^S - d_+^S} \left((L^S - d_+^S) \kappa_-^S + d_+^S \kappa_+^S \right) \quad \text{and} \quad \varphi_+^S = \frac{1}{L^S - d_-^S - d_+^S} \left((L^S - d_-^S) \kappa_+^S + d_-^S \kappa_-^S \right) \quad (25)$$

and the corresponding first-order derivatives with respect to state variables κ^S , cell side length L^S and hinge eccentricities \mathbf{w}^S are

$$\begin{aligned} \frac{\partial \varphi_-^S}{\partial \kappa^S} &= \frac{1}{L^S - d_-^S - d_+^S} \begin{bmatrix} L^S - d_+^S & d_+^S \end{bmatrix}^\top & \frac{\partial \varphi_+^S}{\partial \kappa^S} &= \frac{1}{L^S - d_-^S - d_+^S} \begin{bmatrix} d_-^S & L^S - d_-^S \end{bmatrix}^\top \\ \frac{\partial \varphi_-^S}{\partial \nu^S} &= \frac{1}{L^S - d_-^S - d_+^S} (\kappa_-^S - \varphi_-^S) & \frac{\partial \varphi_+^S}{\partial \nu^S} &= \frac{1}{L^S - d_-^S - d_+^S} (\kappa_+^S - \varphi_+^S) \\ \frac{\partial \varphi_-^S}{\partial \mathbf{w}^S} &= \frac{1}{L^S - d_-^S - d_+^S} \begin{bmatrix} \varphi_-^S & \kappa_+^S - \kappa_-^S + \varphi_+^S \end{bmatrix}^\top & \frac{\partial \varphi_+^S}{\partial \mathbf{w}^S} &= \frac{1}{L^S - d_-^S - d_+^S} \begin{bmatrix} \kappa_-^S - \kappa_+^S + \varphi_-^S & \varphi_+^S \end{bmatrix}^\top. \end{aligned} \quad (26)$$

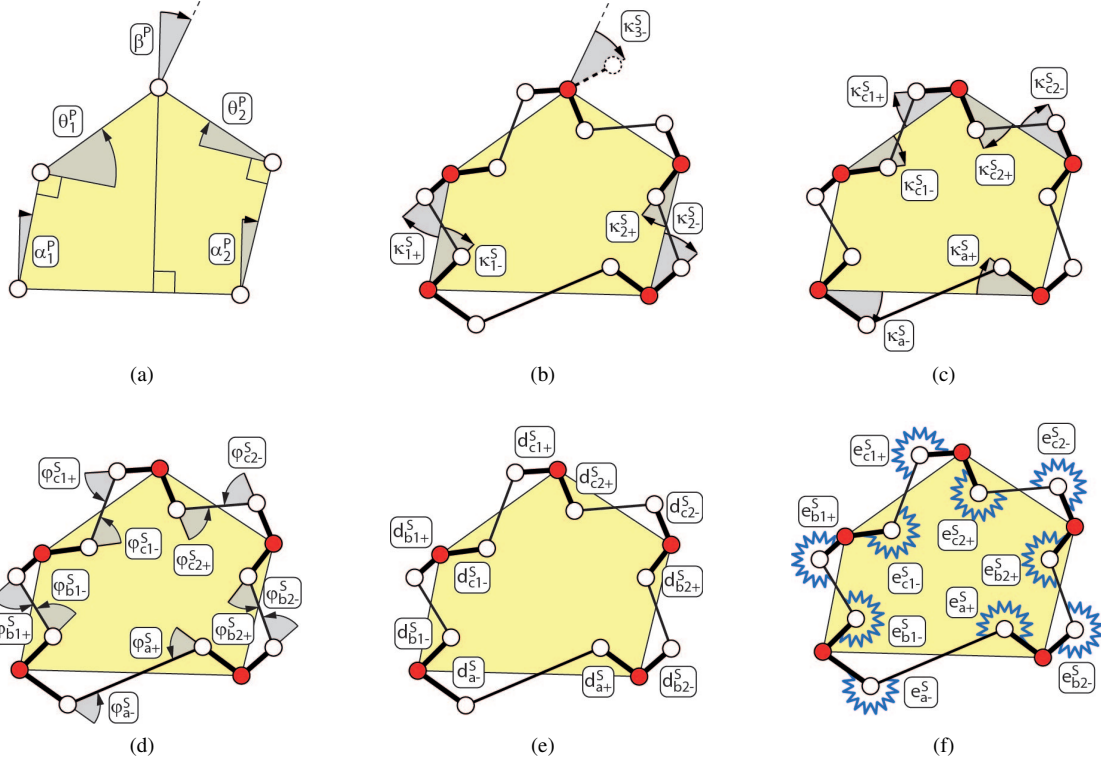


Figure 7: (a) State variables \mathbf{u}_α^P of a pentagonal cell. (b) Global state variables \mathbf{u}_κ for hinge eccentricities are defined with respect to cell sides "b". (c) State variables of sides \mathbf{a}^S and \mathbf{c}^S are a function of global state variables \mathbf{u}_κ and pentagonal state variables \mathbf{u}_α^P . (d) Corresponding bending angles, (e) hinge eccentricities and (f) cell side springs.

4.2 Pressure and Strain Potential

The linearized pressure potential of a cell side due to the differential pressure Δp^S between adjacent cells is

$$\Pi_p^S = -\frac{\Delta p^S}{2} \begin{bmatrix} -d_-^S (L^S - d_+^S) & d_+^S (L^S - d_-^S) \end{bmatrix} \begin{bmatrix} \kappa_-^S \\ \kappa_+^S \end{bmatrix} \quad (27)$$

so that first-order derivatives with respect to state variables κ^S , cell side length L^S and hinge eccentricities \mathbf{d}^S are

$$\begin{aligned} \Pi_p^{S,u_\kappa} &= -\frac{\Delta p^S}{2} \begin{bmatrix} -d_-^S (L^S - d_+^S) & d_+^S (L^S - d_-^S) \end{bmatrix}^\top \\ \Pi_p^{S,v} &= -\frac{\Delta p^S}{2} (d_+^S \kappa_+^S - d_-^S \kappa_-^S) \\ \Pi_p^{S,w} &= -\frac{\Delta p^S}{2} \begin{bmatrix} -(L^S - d_+^S) \kappa_-^S - d_+^S \kappa_+^S & (L^S - d_-^S) \kappa_+^S + d_-^S \kappa_-^S \end{bmatrix}^\top. \end{aligned} \quad (28)$$

The potential of rotational cell side springs is

$$\Pi_e^S = \frac{1}{2} (e_-^S \varphi_-^{S^2} + e_+^S \varphi_+^{S^2}) \quad (29)$$

so that its first-order derivatives with respect to state variables κ^S , cell side length L^S , hinge eccentricities \mathbf{d}^S and springs \mathbf{e}^S are

$$\begin{aligned} \Pi_e^{S,u_\kappa} &= e_-^S \varphi_-^S \frac{\partial \varphi_-^S}{\partial \kappa^S} + e_+^S \varphi_+^S \frac{\partial \varphi_+^S}{\partial \kappa^S} & \Pi_e^{S,v} &= e_-^S \varphi_-^S \frac{\partial \varphi_-^S}{\partial v^S} + e_+^S \varphi_+^S \frac{\partial \varphi_+^S}{\partial v^S} \\ \Pi_e^{S,w} &= e_-^S \varphi_-^S \frac{\partial \varphi_-^S}{\partial \mathbf{w}^S} + e_+^S \varphi_+^S \frac{\partial \varphi_+^S}{\partial \mathbf{w}^S} & \Pi_e^{S,x} &= \frac{1}{2} \begin{bmatrix} \varphi_-^{S^2} & \varphi_+^{S^2} \end{bmatrix}^\top. \end{aligned} \quad (30)$$

The total energy of a cell side is the sum of its pressure and bending energy is

$$\Pi^S = \Pi_p^S + \Pi_e^S \quad (31)$$

and its first-order derivative with respect to local \mathbf{u}_α^P , global β^P pentagonal state variables results in

$$\Pi^{S,u_\alpha} = \Pi^{S,u_\kappa} \left(\frac{\partial \mathbf{u}_\kappa^S}{\partial \mathbf{u}_\alpha^P} \frac{\partial \mathbf{u}_\alpha^P}{\partial \mathbf{u}_\alpha} + \frac{\partial \mathbf{u}_\kappa^S}{\partial \beta^P} \frac{\partial \beta^P}{\partial \mathbf{u}_\alpha} \right). \quad (32)$$

5 Cellular Structure

5.1 State and Optimization Variables

The variables that are used for the description of a cellular structure are summarized in Figure 8. State variables \mathbf{u}_α describe the state of a cellular structure with central cell corner hinges and state variables \mathbf{u}_κ augment the latter to describe hinge eccentricities

$$\begin{aligned} \mathbf{u}_\alpha &= \begin{bmatrix} \alpha_1 & \dots & \alpha_{2n^P} & \beta_{1,1} & \dots & \beta_{n^L-1,n^P-n^L+2} \end{bmatrix}^\top \in \mathbb{R}^{n^\alpha} \\ \mathbf{u}_\kappa &= \begin{bmatrix} \kappa_{1,1-} & \kappa_{1,1+} & \dots & \kappa_{n^L,n^P-n^L+2-} & \kappa_{n^L,n^P-n^L+2+} & \dots & \kappa_{n^L+1,n^P-n^L-} & \kappa_{n^L+1,n^P-n^L+1-} \end{bmatrix}^\top \in \mathbb{R}^{n^\kappa}. \end{aligned} \quad (33)$$

The total state vector of a cellular structure is defined as

$$\mathbf{u} = \begin{bmatrix} \mathbf{u}_\alpha^\top & \mathbf{u}_\kappa^\top \end{bmatrix}^\top \in \mathbb{R}^{n^\alpha + n^\kappa} \quad (34)$$

where the number of state variables n^α and n^κ is

$$n^\alpha = n^C + n^L + n^P - 1 \quad \text{and} \quad n^\kappa = 2n^C + n^L + n^P + 1. \quad (35)$$

Note that n^C is the total number of cells, n^L the number of cell levels and n^P the number of base pentagons. The ratio between state variables of a cellular structure with and without hinge eccentricities is

$$\frac{n^\alpha + n^\kappa}{n^\alpha} = \frac{3n^C + 2n^L + 2n^P}{n^C + n^L + n^P - 1} \quad \text{so that} \quad \lim_{n^P \rightarrow \infty} \frac{n^\alpha + n^\kappa}{n^\alpha} = \frac{3n^L + 2}{n^L + 1} \quad \text{and} \quad \lim_{\substack{n^P \rightarrow \infty \\ n^L \rightarrow \infty}} \frac{n^\alpha + n^\kappa}{n^\alpha} = 3. \quad (36)$$

Therefore, consideration of hinge eccentricities can, depending on the number of base pentagons and cell rows, triple the number of state variables. Side lengths \mathbf{v} , hinge eccentricities \mathbf{w} and rotational springs \mathbf{x}_κ are

$$\begin{aligned} \mathbf{v} &= \begin{bmatrix} \mathbf{b}_1 & \mathbf{c}_1 & \dots & \mathbf{b}_{n^L} & \mathbf{c}_{n^L} & \mathbf{a} \end{bmatrix}^\top \in \mathbb{R}^{n^v} \\ \mathbf{w} &= \begin{bmatrix} d_{b,1-} & d_{b,1+} & \dots & d_{b,n^P+1-} & d_{b,n^P+1+} & \mathbf{d}_{c,1\pm} & \dots & \mathbf{d}_{b,n^L\pm} & \mathbf{d}_{c,n^L\pm} & \mathbf{d}_{a,1\pm} & \dots & \mathbf{d}_{a,n^P\pm} \end{bmatrix}^\top \in \mathbb{R}^{n^w} \\ \mathbf{x}_\kappa &= \begin{bmatrix} e_{b,1-} & e_{b,1+} & \dots & e_{b,n^P+1-} & e_{b,n^P+1+} & \mathbf{e}_{c,1\pm} & \dots & \mathbf{e}_{b,n^L\pm} & \mathbf{e}_{c,n^L\pm} & \mathbf{e}_{a,1\pm} & \dots & \mathbf{e}_{a,n^P\pm} \end{bmatrix}^\top \in \mathbb{R}^{n^{\mathbf{x}}} \end{aligned} \quad (37)$$

so that

$$n^v = 3n^C + n^L + n^P, \quad n^w = 2n^v \quad \text{and} \quad n^{\mathbf{x}\kappa} = 2n^v. \quad (38)$$

Note that cell sides \mathbf{b} are the reference for state variables κ . Furthermore, $\kappa^0 = \mathbf{0}$ since reference sides are assumed to be straight. The total number of pentagonal and hexagonal cells n^C and triangular cells n^T of a cellular structure are

$$n^C = \frac{n^L}{2} (2n^P - n^L + 1) \quad \text{and} \quad n^T = \frac{n^L - 1}{2} (2n^P - n^L). \quad (39)$$

5.2 Model Reduction for Vanishing Hinge Eccentricities

The numerical model can be simplified if hinge eccentricities vanish so that cell corner hinges coincide as shown in Figure 9. Contributions to the pressure potential from cell sides are zero for $\mathbf{w} = \mathbf{0}$ and bending angles reduce to

$$\begin{bmatrix} \varphi_1 \\ \varphi_2 \\ \varphi_3 \end{bmatrix} = \begin{bmatrix} 0 & 0 \\ 0 & 1 \\ -1 & 0 \end{bmatrix} \begin{bmatrix} \Delta\alpha_1 \\ \Delta\alpha_2 \end{bmatrix} - \begin{bmatrix} 1 \\ 1 \\ 1 \end{bmatrix} \kappa \quad (40)$$

where $\Delta\alpha = \alpha - \alpha^0$. The total bending energy

$$\Pi_e = \frac{1}{2} (e_1 \varphi_1^2 + e_2 \varphi_2^2 + e_3 \varphi_3^2) \quad \text{is minimal for} \quad \kappa = \frac{1}{e_1 + e_2 + e_3} \begin{bmatrix} -e_3 & e_2 \end{bmatrix} \begin{bmatrix} \Delta\alpha_1 \\ \Delta\alpha_2 \end{bmatrix} \quad (41)$$

so that angles φ are

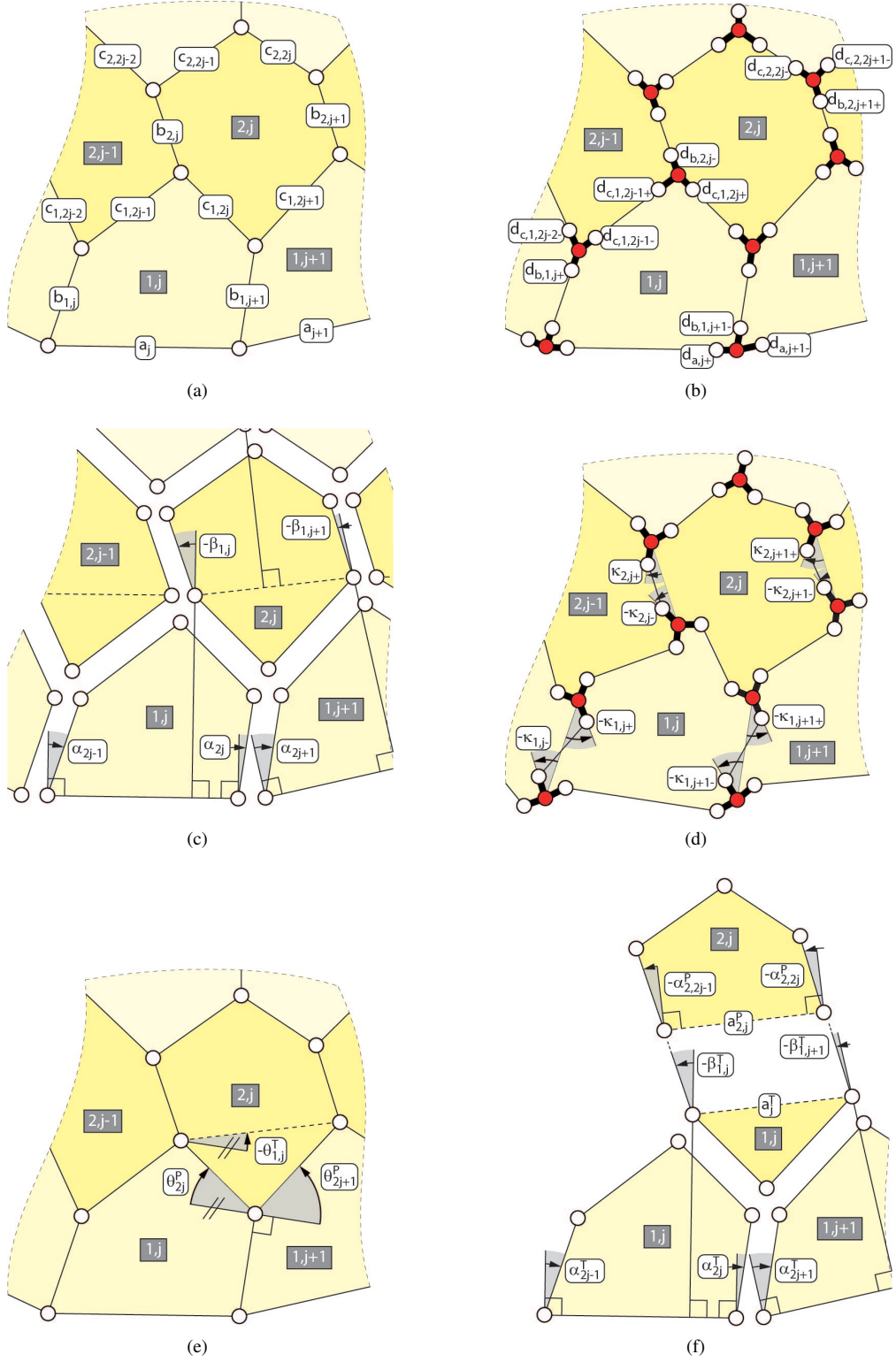


Figure 8: Geometric variables of a cellular structure with eccentric cell corner hinges. (a) Side lengths and (b) hinge eccentricities. State variables for (c) rigid body and (d) deformational motion. (e) Internal angles and (f) state variables of a hexagonal cell.

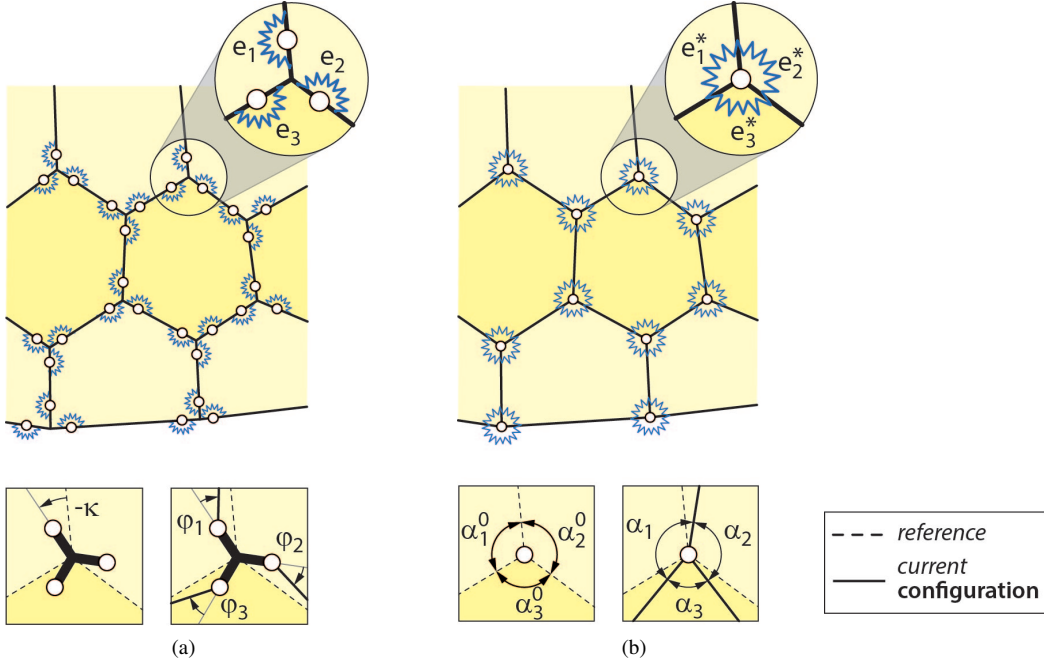


Figure 9: Numerical model and cell corner angles for (a) finite and (b) zero hinge eccentricities.

$$\begin{bmatrix} \varphi_1 \\ \varphi_2 \\ \varphi_3 \end{bmatrix} = \frac{1}{e_1 + e_2 + e_3} \begin{bmatrix} e_3 & -e_2 \\ e_3 & e_1 + e_3 \\ -e_1 - e_2 & -e_2 \end{bmatrix} \begin{bmatrix} \Delta\alpha_1 \\ \Delta\alpha_2 \end{bmatrix}. \quad (42)$$

The bending energy Π_e becomes

$$\Pi_e = \frac{1}{2(e_1 + e_2 + e_3)} (e_3 e_1 \Delta\alpha_1^2 + e_1 e_2 \Delta\alpha_2^2 + e_2 e_3 \Delta\alpha_3^2) \quad (43)$$

where $\Delta\alpha_3 = \Delta\alpha_1 + \Delta\alpha_2$. Hence it is possible to derive a set of cell corner springs that are energetically conjugate to cell corner angles α so that

$$\begin{bmatrix} e_1^* & e_2^* & e_3^* \end{bmatrix}^\top = \frac{1}{e_1 + e_2 + e_3} \begin{bmatrix} e_3 e_1 & e_1 e_2 & e_2 e_3 \end{bmatrix}^\top. \quad (44)$$

Therefore it is possible to eliminate state variables \mathbf{u}_x if $\mathbf{w} = \mathbf{0}$ and thus to significantly simplify the numerical model. Furthermore, the presented framework reduces to the numerical model introduced in [11] if hinge eccentricities and rotational springs are zero.

5.3 Transformation Matrices

State variables $\mathbf{u}_{\alpha,i+1,j}^p$ of the j -th pentagonal cell in the $i+1$ -th cell row can be expressed in terms of local $\mathbf{u}_{\alpha,i,j}^T$, global $\beta_{i,j}^T$ state and optimization $\mathbf{v}_{i,j}^T$ variables of the j -th triangular cell in the i -th cell row as shown in Figure 8 so that

$$\mathbf{u}_{\alpha,i+1}^P (\mathbf{u}_{\alpha,i}^T, \boldsymbol{\beta}_i^T) = \begin{bmatrix} \alpha_{1,i+1,j}^P & \alpha_{2,i+1,j}^P & \alpha_{i+1,j}^P \end{bmatrix}^T = \begin{bmatrix} \beta_{1,i,j}^T - \alpha_{2,i,j}^T - \theta_{i,j}^T & \beta_{2,i,j}^T - \alpha_{3,i,j}^T - \theta_{i,j}^T & a_{i,j}^T \end{bmatrix}^T. \quad (45)$$

Transformation matrix $\mathbf{T}_{i,j}^\beta$ relates state variables of a pentagonal cell to global state variables $\boldsymbol{\beta}^T$ of a triangular cell

$$\mathbf{T}_{i,j}^\beta = \frac{\partial \mathbf{u}_{\alpha,i+1,j}^P}{\partial \boldsymbol{\beta}_{i,j}^T} = \begin{bmatrix} 1 & 0 & 0 \\ 0 & 1 & 0 \end{bmatrix} \quad (46)$$

and $\mathbf{T}_{i,j}^{\mathbf{u}_\alpha}$ relates pentagonal to triangular state variables so that

$$\mathbf{T}_{i,j}^{\mathbf{u}_\alpha} = \frac{\partial \mathbf{u}_{\alpha,i+1,j}^P}{\partial \mathbf{u}_{\alpha,i,j}^T} = \begin{bmatrix} -\frac{\partial \theta_{i,j}^T}{\partial \alpha_{1,i,j}^T} & -1 - \frac{\partial \theta_{i,j}^T}{\partial \alpha_{2,i,j}^T} & -\frac{\partial \theta_{i,j}^T}{\partial \alpha_{3,i,j}^T} & -\frac{\partial \theta_{i,j}^T}{\partial \alpha_{4,i,j}^T} & -\frac{\partial \theta_{i,j}^T}{\partial a_{1,i,j}^T} & -\frac{\partial \theta_{i,j}^T}{\partial a_{2,i,j}^T} \\ \frac{\partial \theta_{i,j}^T}{\partial \alpha_{1,i,j}^T} & \frac{\partial \theta_{i,j}^T}{\partial \alpha_{2,i,j}^T} & -1 - \frac{\partial \theta_{i,j}^T}{\partial \alpha_{3,i,j}^T} & -\frac{\partial \theta_{i,j}^T}{\partial \alpha_{4,i,j}^T} & -\frac{\partial \theta_{i,j}^T}{\partial a_{1,i,j}^T} & -\frac{\partial \theta_{i,j}^T}{\partial a_{2,i,j}^T} \\ -\frac{\partial \alpha_{1,i,j}^T}{\partial a_{1,i,j}^T} & -\frac{\partial \alpha_{2,i,j}^T}{\partial a_{1,i,j}^T} & -\frac{\partial \alpha_{3,i,j}^T}{\partial a_{1,i,j}^T} & -\frac{\partial \alpha_{4,i,j}^T}{\partial a_{1,i,j}^T} & \frac{\partial a_{1,i,j}^T}{\partial a_{1,i,j}^T} & \frac{\partial a_{2,i,j}^T}{\partial a_{1,i,j}^T} \\ \frac{\partial \alpha_{1,i,j}^T}{\partial a_{2,i,j}^T} & \frac{\partial \alpha_{2,i,j}^T}{\partial a_{2,i,j}^T} & \frac{\partial \alpha_{3,i,j}^T}{\partial a_{2,i,j}^T} & \frac{\partial \alpha_{4,i,j}^T}{\partial a_{2,i,j}^T} & \frac{\partial a_{1,i,j}^T}{\partial a_{2,i,j}^T} & \frac{\partial a_{2,i,j}^T}{\partial a_{2,i,j}^T} \end{bmatrix}^T. \quad (47)$$

Similarly, $\mathbf{T}_{i,j}^{\mathbf{v}}$ links state variables of a pentagonal cell to triangular cell side lengths

$$\mathbf{T}_{i,j}^{\mathbf{v}} = \frac{\partial \mathbf{u}_{\alpha,i+1,j}^P}{\partial \mathbf{v}_{i,j}^T} = \begin{bmatrix} -\frac{\partial \theta_{i,j}^T}{\partial b_{1,i,j}^T} & -\frac{\partial \theta_{i,j}^T}{\partial b_{2,i,j}^T} & -\frac{\partial \theta_{i,j}^T}{\partial b_{3,i,j}^T} & -\frac{\partial \theta_{i,j}^T}{\partial c_{1,i,j}^T} & -\frac{\partial \theta_{i,j}^T}{\partial c_{2,i,j}^T} & -\frac{\partial \theta_{i,j}^T}{\partial c_{3,i,j}^T} & -\frac{\partial \theta_{i,j}^T}{\partial c_{4,i,j}^T} \\ \frac{\partial \theta_{i,j}^T}{\partial b_{1,i,j}^T} & \frac{\partial \theta_{i,j}^T}{\partial b_{2,i,j}^T} & \frac{\partial \theta_{i,j}^T}{\partial b_{3,i,j}^T} & -\frac{\partial \theta_{i,j}^T}{\partial c_{1,i,j}^T} & -\frac{\partial \theta_{i,j}^T}{\partial c_{2,i,j}^T} & -\frac{\partial \theta_{i,j}^T}{\partial c_{3,i,j}^T} & -\frac{\partial \theta_{i,j}^T}{\partial c_{4,i,j}^T} \\ -\frac{\partial b_{1,i,j}^T}{\partial a_{1,i,j}^T} & -\frac{\partial b_{2,i,j}^T}{\partial a_{1,i,j}^T} & -\frac{\partial b_{3,i,j}^T}{\partial a_{1,i,j}^T} & -\frac{\partial c_{1,i,j}^T}{\partial a_{1,i,j}^T} & -\frac{\partial c_{2,i,j}^T}{\partial a_{1,i,j}^T} & -\frac{\partial c_{3,i,j}^T}{\partial a_{1,i,j}^T} & -\frac{\partial c_{4,i,j}^T}{\partial a_{1,i,j}^T} \\ \frac{\partial b_{1,i,j}^T}{\partial a_{2,i,j}^T} & \frac{\partial b_{2,i,j}^T}{\partial a_{2,i,j}^T} & \frac{\partial b_{3,i,j}^T}{\partial a_{2,i,j}^T} & \frac{\partial c_{1,i,j}^T}{\partial a_{2,i,j}^T} & \frac{\partial c_{2,i,j}^T}{\partial a_{2,i,j}^T} & \frac{\partial c_{3,i,j}^T}{\partial a_{2,i,j}^T} & \frac{\partial c_{4,i,j}^T}{\partial a_{2,i,j}^T} \end{bmatrix}^T. \quad (48)$$

Transformation matrices for reference state variables are derived in a similar manner and denoted as, for example, $\mathbf{T}_{i,j}^0$. Corresponding higher order transformation matrices are

$$\mathbf{T}_{i,j}^{\mathbf{u}_\alpha \mathbf{u}_\alpha} = \frac{\partial^2 \mathbf{u}_{\alpha,i+1,j}^P}{\partial \mathbf{u}_{\alpha,i,j}^T{}^2}, \quad \mathbf{T}_{i,j}^{\mathbf{u}_\alpha \mathbf{v}} = \frac{\partial^2 \mathbf{u}_{\alpha,i+1,j}^P}{\partial \mathbf{u}_{\alpha,i,j}^T \partial \mathbf{v}_{i,j}^T} \quad \text{and} \quad \mathbf{T}_{i,j}^{\mathbf{v} \mathbf{v}} = \frac{\partial^2 \mathbf{u}_{\alpha,i+1,j}^P}{\partial \mathbf{v}_{i,j}^T{}^2}. \quad (49)$$

5.4 Potential Energy

The potential energy of a cellular structure is

$$\Pi = \sum_{i=1}^{n^L} \left(\sum_{j=1}^{n^P+2-i} \Pi_{b,i,j}^S + \sum_{j=1}^{n^P+1-i} \left(\Pi_{i,j}^P + \delta_i^1 \Pi_{a,j}^S + \Pi_{c,i,2j-1}^S + \Pi_{c,i,2j}^S \right) + \left(1 - \delta_i^{n^L} \right) \sum_{j=1}^{n^P-i} \Pi_{i,j}^T \right) \quad (50)$$

where $\delta_i^{n^L}$ is a Kronecker delta. Required derivatives for the simulation and optimization of pressure actuated cellular structures are summarized in Figure 10. The first-order derivative $\boldsymbol{\Pi}^{\mathbf{u}} \in \mathbb{R}^{n^u+n^k}$ is subsequently used to outline the assembly process. The derivative $\boldsymbol{\Pi}_i^{\mathbf{u}}$ of the i -th cell row is

$$\begin{aligned}
\Pi_i^u = & \sum_{j=1}^{n^p+2-i} \left(\Pi_{b,i,j}^{S,u_\alpha} \frac{\partial \mathbf{u}_{\alpha,i,j}^S}{\partial \mathbf{u}_i} + \Pi_{b,i,j}^{S,u_\kappa} \frac{\partial \mathbf{u}_{\kappa,i,j}^S}{\partial \mathbf{u}_i} \right) \\
& + \sum_{j=1}^{n^p+1-i} \left(\Pi_{i,j}^{P,u_\alpha} \frac{\partial \mathbf{u}_{\alpha,i,j}^P}{\partial \mathbf{u}_i} + \delta_i^1 \left(\Pi_{a,i,j}^{S,u_\alpha} \frac{\partial \mathbf{u}_{\alpha,i,j}^S}{\partial \mathbf{u}_i} + \Pi_{a,i,j}^{S,u_\kappa} \frac{\partial \mathbf{u}_{\kappa,i,j}^S}{\partial \mathbf{u}_i} \right) + \left(\Pi_{c,i,2j-1}^{S,u_\alpha} + \Pi_{c,i,2j}^{S,u_\alpha} \right) \frac{\partial \mathbf{u}_{\alpha,i,j}^S}{\partial \mathbf{u}_i} + \left(\Pi_{c,i,2j-1}^{S,u_\kappa} + \Pi_{c,i,2j}^{S,u_\kappa} \right) \frac{\partial \mathbf{u}_{\kappa,i,j}^S}{\partial \mathbf{u}_i} \right) \\
& + (1 - \delta_i^{n^L}) \sum_{j=1}^{n^p-i} \Pi_{i,j}^{T,u_\alpha} \frac{\partial \mathbf{u}_{\alpha,i,j}^T}{\partial \mathbf{u}_i}
\end{aligned} \tag{51}$$

where \mathbf{u}_i are the state variables of a cellular structure that consists only of cell rows $[i, n^L]$. Adding and transforming the derivatives of single cell rows from top to bottom leads to

$$\Pi^u = \left(\left(\Pi_{n^L}^u \frac{\partial \mathbf{u}_{n^L}}{\partial \mathbf{u}_{n^L-1}} + \dots + \Pi_4^u \right) \frac{\partial \mathbf{u}_4}{\partial \mathbf{u}_3} + \Pi_3^u \right) \frac{\partial \mathbf{u}_3}{\partial \mathbf{u}_2} + \Pi_2^u \frac{\partial \mathbf{u}_2}{\partial \mathbf{u}_1} + \Pi_1^u \tag{52}$$

where terms such as $\partial \mathbf{u}_{i+1} / \partial \mathbf{u}_i$ are assembled from previously introduced transformation matrices \mathbf{T} . It should be noted that derivatives with respect to cell side lengths \mathbf{v} depend on the current and reference configuration. Virtual derivatives such as Π_{vir}^v are used for the computation of axial cell side forces. Therefore, reference terms are neglected in their construction.

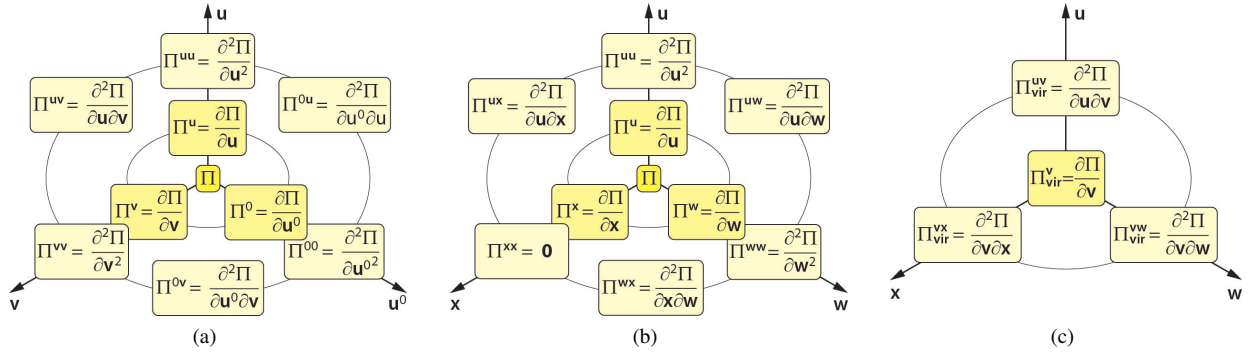


Figure 10: Required derivatives of potential energy with respect to state variables \mathbf{u}_0 , \mathbf{u} , cell side lengths \mathbf{v} , hinge eccentricities \mathbf{w} and springs \mathbf{x} .

5.5 Equilibrium Configurations

The Newton-Raphson method is used to compute the equilibrium for a given reference configuration and pressure set q . Current state variables of the $i + 1$ -th iteration are

$$\mathbf{u}_q^{i+1} = \mathbf{u}_q^i - (\Pi_q^{uu})^{-1} \Pi_q^u. \tag{53}$$

Pressure actuated cellular structures with n^L cell rows are usually designed for n^L target shapes that are associated to n^L pressure sets. An optimal reference configuration minimizes the overall energy of the n^L current configurations so that optimal reference state variables for the $i + 1$ -th iteration are

$$\mathbf{u}_0^{i+1} = \mathbf{u}_0^i - \left(\sum_{q=1}^{n^L} \mathbf{\Pi}_q^{00} \right)^{-1} \sum_{q=1}^{n^L} \mathbf{\Pi}_q^0. \quad (54)$$

It should be noted that the influence of reference state variables \mathbf{u}_0 on current state variables \mathbf{u}_q for the q -th pressure set is

$$\mathbf{G}_q^0 = - \left(\mathbf{\Pi}_q^{uu} \right)^{-1} \mathbf{\Pi}_q^{0u^\top}. \quad (55)$$

5.6 Gradient Based Optimization

Side lengths of pressure actuated cellular structures with n^L cell rows can be optimized for n^L pressure sets such that their outer pentagonal cell corners are located on n^L different C^1 continuous functions. These target shapes are defined by angles between pentagonal base sides so that for the q -th pressure set

$$\Delta\alpha_{q,j} = \alpha_{q,2j} - \alpha_{q,2j+1} \quad \text{for} \quad j \in [1, n^P - 1]. \quad (56)$$

The gradient matrix \mathbf{G}_q^v that relates current state variables of the q -th pressure set to cell side lengths \mathbf{v} is

$$\mathbf{G}_q^v = - \left(\mathbf{\Pi}_q^{uu} \right)^{-1} \mathbf{\Pi}_q^{uv} = \begin{bmatrix} \frac{\partial\alpha_{1,q}}{\partial b_{1,1}} & \cdots & \frac{\partial\alpha_{1,q}}{\partial c_{n^L,2(n^P-n^L+1)}} \\ \vdots & \ddots & \vdots \\ \frac{\partial\beta_{1,q}}{\partial b_{1,1}} & \cdots & \frac{\partial\beta_{1,q}}{\partial c_{n^L,2(n^P-n^L+1)}} \end{bmatrix}. \quad (57)$$

The single matrices \mathbf{G}_q^v can be assembled into a gradient matrix \mathbf{G}^v that relates the change of target angles to optimization variables for all pressure sets

$$\mathbf{G}^v = \begin{bmatrix} \frac{\partial\alpha_{2,1}}{\partial b_{1,1}} - \frac{\partial\alpha_{3,1}}{\partial b_{1,1}} & \cdots & \frac{\partial\alpha_{2n^P-2,1}}{\partial b_{1,1}} - \frac{\partial\alpha_{2n^P-1,1}}{\partial b_{1,1}} & \left| \begin{array}{c} \frac{\partial\alpha_{2,n^L}}{\partial b_{1,1}} - \frac{\partial\alpha_{3,n^L}}{\partial b_{1,1}} & \cdots & \frac{\partial\alpha_{2n^P-2,n^L}}{\partial b_{1,1}} - \frac{\partial\alpha_{2n^P-1,n^L}}{\partial b_{1,1}} \end{array} \right|^\top \\ \vdots & \ddots & \vdots & \vdots \\ \frac{\partial\alpha_{2,1}}{\partial c_{n^L,X}} - \frac{\partial\alpha_{3,1}}{\partial c_{n^L,X}} & \cdots & \frac{\partial\alpha_{2n^P-2,1}}{\partial c_{n^L,X}} - \frac{\partial\alpha_{2n^P-1,1}}{\partial c_{n^L,X}} & \left| \begin{array}{c} \frac{\partial\alpha_{2,n^L}}{\partial c_{n^L,X}} - \frac{\partial\alpha_{3,n^L}}{\partial c_{n^L,X}} & \cdots & \frac{\partial\alpha_{2n^P-2,n^L}}{\partial c_{n^L,X}} - \frac{\partial\alpha_{2n^P-1,n^L}}{\partial c_{n^L,X}} \end{array} \right|^\top \end{bmatrix} \quad (58)$$

where $X = 2(n^P - n^L + 1)$. Note that \mathbf{G}^v is not quadratic and thus not invertible. The fact that \mathbf{G}^v possesses more columns than rows indicates that an optimized structure is not unique. The residual vector \mathbf{r} is the difference between current and target angles at outer pentagonal cell corners for all pressure sets so that

$$\mathbf{r} = \left[\Delta\alpha_{1,1} - (\alpha_{2,1} - \alpha_{3,1}) \cdots \Delta\alpha_{n^P-1,n^L} - (\alpha_{2n^P-2,n^L} - \alpha_{2n^P-1,n^L}) \right]^\top \quad (59)$$

where $\Delta\alpha_{j,q}$ is the target angle between the j and $j+1$ -th pentagonal cell for the q -th pressure set. The gradient vector \mathbf{g} relates the change of the residual vector \mathbf{r} to the change of cell sides \mathbf{v}

$$\mathbf{g} = \mathbf{G}^{v^\top} \mathbf{r} \quad (60)$$

and the updated cell sides for the $i + 1$ -th iteration during an optimization are

$$\mathbf{v}^{i+1} = \mathbf{v}^i + \lambda \mathbf{g} \quad (61)$$

where λ is an unknown multiplier. The Euclidean norm of the linearly extrapolated residuum vector \mathbf{r}^{i+1}

$$\mathbf{r}^{i+1} = \mathbf{r}^i - \mathbf{G}^v \Delta \mathbf{v} = \mathbf{r}^i - \lambda \mathbf{G}^v \mathbf{g} \quad (62)$$

is minimal for

$$\lambda = \frac{\mathbf{g}^\top \mathbf{g}}{\mathbf{g}^\top \mathbf{G}^{v\top} \mathbf{G}^v \mathbf{g}}. \quad (63)$$

Constraining cell side lengths during an optimization is necessary to prevent small or unbalanced cells. This can be done by setting the corresponding entries in the gradient vectors \mathbf{g} to zero before computing λ .

5.7 Potential Based Optimization

The gradient based optimization approach has the drawback that it requires a large number of iterations. This problem can be overcome by using a second-order approach. A potential Π_{opt} is defined as

$$\Pi_{\text{opt}} = \sum_{i=1}^{n^L-1} \sum_{j=i+1}^{n^L} (\eta_{ij} \Pi_i - \eta_{ji} \Pi_j)^2 \quad (64)$$

where η are weighting factors and Π_i is the potential of the i -th pressure set. It can be seen that the potentials of all current configurations are weighted and subtracted from each other to create a global potential. It should be noted that the definition of the potential is arbitrary and the only requirement is that it has a minimum (preferably only one). The first-order derivative with respect to cell sides \mathbf{v} is

$$\mathbf{\Pi}_{\text{opt}}^v = 2 \sum_{i=1}^{n^L-1} \sum_{j=i+1}^{n^L} (\eta_{ij} \Pi_i - \eta_{ji} \Pi_j) \left(\eta_{ij} \frac{\partial \Pi_i}{\partial \mathbf{v}} - \eta_{ji} \frac{\partial \Pi_j}{\partial \mathbf{v}} \right) \quad (65)$$

where

$$\frac{\partial \Pi_q}{\partial \mathbf{v}} = \mathbf{G}_q^{v\top} \mathbf{\Pi}_q^u + \mathbf{\Pi}_q^v. \quad (66)$$

Note that state variables \mathbf{u} are eliminated by using the gradient matrix \mathbf{G}^v . The corresponding second-order derivative is

$$\mathbf{\Pi}_{\text{opt}}^{vv} = 2 \sum_{i=1}^{n^L-1} \sum_{j=i+1}^{n^L} \left(\left(\eta_{ij} \frac{\partial \Pi_i}{\partial \mathbf{v}} - \eta_{ji} \frac{\partial \Pi_j}{\partial \mathbf{v}} \right) \left(\eta_{ij} \frac{\partial \Pi_i}{\partial \mathbf{v}} - \eta_{ji} \frac{\partial \Pi_j}{\partial \mathbf{v}} \right)^\top + (\eta_{ij} \Pi_i - \eta_{ji} \Pi_j) \left(\eta_{ij} \frac{\partial^2 \Pi_i}{\partial \mathbf{v}^2} - \eta_{ji} \frac{\partial^2 \Pi_j}{\partial \mathbf{v}^2} \right) \right) \quad (67)$$

where

$$\frac{\partial^2 \Pi_q}{\partial \mathbf{v}^2} = \frac{\partial \mathbf{G}_q^{v\top}}{\partial \mathbf{v}} \mathbf{\Pi}_q^u + \mathbf{G}_q^{v\top} \mathbf{\Pi}_q^{uu} \mathbf{G}_q^v + \mathbf{G}_q^{v\top} \mathbf{\Pi}_q^{uv} + \mathbf{\Pi}_q^{uv\top} \mathbf{G}_q^v + \mathbf{\Pi}_q^{vv}. \quad (68)$$

Previous equations reduce to

$$\frac{\partial \Pi_q}{\partial \mathbf{v}} = \Pi_q^{\mathbf{v}} \quad \text{and} \quad \frac{\partial^2 \Pi_q}{\partial \mathbf{v}^2} = \mathbf{G}_q^{\mathbf{v}\top} \Pi_q^{\mathbf{uu}} \mathbf{G}_q^{\mathbf{v}} + \mathbf{G}_q^{\mathbf{v}\top} \Pi_q^{\mathbf{uv}} + \Pi_q^{\mathbf{uv}\top} \mathbf{G}_q^{\mathbf{v}} + \Pi_q^{\mathbf{vv}}. \quad (69)$$

since $\Pi^{\mathbf{u}} = \mathbf{0}$ at an equilibrium configuration. The resulting linear system of equations

$$\mathbf{v}_{\text{aug}}^{i+1} = \mathbf{v}_{\text{aug}}^i - \left(\Pi_{\text{opt,aug}}^{\mathbf{vv}} \right)^{-1} \Pi_{\text{opt,aug}}^{\mathbf{v}} \quad (70)$$

is augmented with Lagrange multipliers for the target shapes $\lambda_{\mathbf{g}}$ and potential cell side constraints $\lambda_{\mathbf{c}}$ so that

$$\Pi_{\text{opt,aug}}^{\mathbf{vv}} = \begin{bmatrix} \Pi_{\text{opt}}^{\mathbf{vv}} & \mathbf{G}^{\mathbf{v}\top} & \mathbf{C}^{\top} \\ \mathbf{G}^{\mathbf{v}} & \mathbf{0} & \mathbf{0} \\ \mathbf{C} & \mathbf{0} & \mathbf{0} \end{bmatrix} \quad \text{and} \quad \Pi_{\text{opt,aug}}^{\mathbf{v}} = \begin{bmatrix} \Pi_{\text{opt}}^{\mathbf{v}} \\ \Delta \alpha \\ \mathbf{0} \end{bmatrix}. \quad (71)$$

Note that the nonlinear constraint $\mathbf{G}^{\mathbf{v}}$ is treated as if it is linear to avoid the computation of third-order derivatives. Furthermore, it should be realized that this approach requires prior knowledge of weighting factors η . Hence it is best to precondition the optimization problem with the gradient based approach and to estimate feasible weighting factors at a later stage. The combination of the gradient and potential based approach as well as the convergence for a linear constraint $\mathbf{G}^{\mathbf{v}}$ are demonstrated in Section 8 by means of several examples.

6 Axial Cell Side Strains

6.1 Additional State Variables

We have previously used cell side lengths \mathbf{v} as optimization variables and assumed that they are invariant to state variables and cell pressures. Consideration of axial strains requires a split into reference \mathbf{v}^0 and current \mathbf{v} side lengths

$$\mathbf{v} = \mathbf{v}^0 + \Delta \mathbf{v} \quad (72)$$

where $\Delta \mathbf{v}$ are cell side elongations due to cell pressures. Hence, side lengths \mathbf{v}^0 are the optimization variables whereas $\Delta \mathbf{v}$ is a function of axial cell side forces $\Pi_{\text{vir}}^{\mathbf{v}}$. The elongation of a single cell side with an axial stiffness h is

$$\Delta v = \frac{v^0}{hS} \Pi_{\text{vir}}^{\mathbf{v}} \quad (73)$$

if engineering strains are assumed. The corresponding axial strain energy is

$$\Pi_h^{\mathbf{S}} = \frac{1}{2} \frac{v^0}{hS} \Pi_{\text{vir}}^{\mathbf{v}^2}. \quad (74)$$

It can be seen that the second-order derivative of the axial strain energy of a single cell side requires third-order derivatives of the potential energy of a cellular structure. This can be avoided by introducing additional state variables

$$\mathbf{u}_h = \begin{bmatrix} \Delta \mathbf{b}_1 & \Delta \mathbf{c}_1 & \dots & \Delta \mathbf{b}_{n^L} & \Delta \mathbf{c}_{n^L} & \Delta \mathbf{a} \end{bmatrix}^{\top} \in \mathbb{R}^{n^w} \quad (75)$$

so that

$$\Pi_h^S = \frac{1}{2} \frac{h^S}{v^0} \Delta v^2. \quad (76)$$

The first-order derivatives with respect to reference length v^0 and side elongation Δv are

$$\Pi_h^{S,v^0} = -\frac{1}{2} \frac{h^S}{v^{0^2}} \Delta v^2 \quad \text{and} \quad \Pi_h^{S,\Delta v} = \frac{h^S}{v^0} \Delta v. \quad (77)$$

Note that this is a tradeoff between the assembly of third-order derivatives and the introduction of additional state variables. It was found that the assembly of third-order derivatives is cumbersome and computationally more expensive than the solution of a linear system with additional degrees of freedom. The potential energy of a cellular structure with axial cell side springs is

$$\Pi = \Pi^P + \Pi_p^S + \Pi_e^S + \Pi_h^S \quad (78)$$

so that its first-order derivatives with respect to state variables \mathbf{u} and cell side elongations $\Delta \mathbf{v}$ are

$$\begin{bmatrix} \Pi^{\mathbf{u}} \\ \Pi^{\Delta \mathbf{v}} \end{bmatrix} = \begin{bmatrix} \Pi^{P,\mathbf{u}} + \Pi_p^{S,\mathbf{u}} + \Pi_e^{S,\mathbf{u}} \\ \Pi_{\text{vir}}^{P,v} + \Pi_{p,\text{vir}}^{S,v} + \Pi_{e,\text{vir}}^{S,v} + \Pi_h^{S,\Delta v} \end{bmatrix}. \quad (79)$$

The equilibrium configurations of a cellular structure for given cell pressures can be computed with the Newton-Raphson method so that

$$\begin{bmatrix} \mathbf{u}_{i+1} \\ \mathbf{v}_{i+1} \end{bmatrix} = \begin{bmatrix} \mathbf{u}_i \\ \mathbf{v}_i \end{bmatrix} - \begin{bmatrix} \Pi^{\mathbf{u}\mathbf{u}} & \Pi^{\mathbf{u}\Delta \mathbf{v}} \\ \Pi^{\mathbf{u}\Delta \mathbf{v}^T} & \Pi^{\Delta \mathbf{v}\Delta \mathbf{v}} \end{bmatrix}^{-1} \begin{bmatrix} \Pi^{\mathbf{u}} \\ \Pi^{\Delta \mathbf{v}} \end{bmatrix}. \quad (80)$$

6.2 Elimination of Axial Degrees of Freedom

It was shown that third-order derivatives can be avoided if additional state variables are used. These additional degrees of freedom vanish at an equilibrium configuration so that they are not required for the optimization. Cell side elongations of a cellular structure are

$$\Delta \mathbf{v} = \begin{bmatrix} v_1^0 & & v_{n^v}^0 \\ \frac{h_1^S}{h_1^S} \Pi_{\text{vir},1}^v & \cdots & \frac{h_{n^v}^S}{h_{n^v}^S} \Pi_{\text{vir},n^v}^v \end{bmatrix}^T \quad (81)$$

and the first-order derivatives with respect to state variables \mathbf{u} , reference side lengths \mathbf{v}^0 are

$$\frac{\partial \Delta \mathbf{v}}{\partial \mathbf{u}} = \mathbf{A}^{-1} \mathbf{B}_{\mathbf{u}} \quad \text{and} \quad \frac{\partial \Delta \mathbf{v}}{\partial \mathbf{v}^0} = \mathbf{A}^{-1} \mathbf{B}_{\mathbf{v}^0} \quad (82)$$

where

$$\mathbf{A} = \begin{bmatrix} 1 - \frac{v_1^0}{h_1^S} \Pi_{\text{vir},1,1}^{vv} & \cdots & -\frac{v_1^0}{h_1^S} \Pi_{\text{vir},1,n^v}^{vv} \\ \vdots & \ddots & \vdots \\ -\frac{v_{n^v}^0}{h_{n^v}^S} \Pi_{\text{vir},n^v,1}^{vv} & \cdots & 1 - \frac{v_{n^v}^0}{h_{n^v}^S} \Pi_{\text{vir},n^v,n^v}^{vv} \end{bmatrix} = \text{diag}(\mathbf{1}) - \text{diag}(\mathbf{v}_1) \Pi_{\text{vir}}^{vv} \quad (83)$$

and

$$\mathbf{B}_u = \begin{bmatrix} \frac{v_1^0}{h_1^S} \Pi_{\text{vir},1,1}^{uv} & \cdots & \frac{v_1^0}{h_1^S} \Pi_{\text{vir},n^u,1}^{uv} \\ \vdots & \ddots & \vdots \\ \frac{v_{n^v}^0}{h_{n^v}^S} \Pi_{\text{vir},1,n^v}^{uv} & \cdots & \frac{v_{n^v}^0}{h_{n^v}^S} \Pi_{\text{vir},n^u,n^v}^{uv} \end{bmatrix} = \text{diag}(\mathbf{v}_1) \mathbf{\Pi}_{\text{vir}}^{uv^\top}$$

$$\mathbf{B}_{v^0} = \begin{bmatrix} \frac{1}{h_1^S} (\Pi_{\text{vir},1}^v + v_1^0 \Pi_{\text{vir},1,1}^{vv}) & \cdots & \frac{v_1^0}{h_1^S} \Pi_{\text{vir},1,n^v}^{vv} \\ \vdots & \ddots & \vdots \\ \frac{v_{n^v}^0}{h_{n^v}^S} \Pi_{\text{vir},n^v,1}^{vv} & \cdots & \frac{1}{h_{n^v}^S} (\Pi_{\text{vir},n^v}^v + v_{n^v}^0 \Pi_{\text{vir},n^v,n^v}^{vv}) \end{bmatrix} = \text{diag}(\mathbf{v}_1) \mathbf{\Pi}_{\text{vir}}^{vv} + \text{diag}(\mathbf{v}_2) \text{diag}(\mathbf{\Pi}_{\text{vir}}^v).$$

Note that

$$\mathbf{v}_1 = \begin{bmatrix} \frac{v_1^0}{h_1^S} & \cdots & \frac{v_{n^v}^0}{h_{n^v}^S} \end{bmatrix}^\top \quad \text{and} \quad \mathbf{v}_2 = \begin{bmatrix} \frac{1}{h_1^S} & \cdots & \frac{1}{h_{n^v}^S} \end{bmatrix}^\top. \quad (84)$$

Therefore, first-order derivatives of the potential energy of a cellular structure with respect to state variables \mathbf{u} and reference cell side lengths \mathbf{v}^0 at an equilibrium configuration can be written as

$$\mathbf{\Pi}_{\text{opt}}^u = \mathbf{\Pi}^u + \frac{\partial \Delta \mathbf{v}^\top}{\partial \mathbf{u}} \mathbf{\Pi}^{\Delta v} = \mathbf{0} \quad \text{and} \quad \mathbf{\Pi}_{\text{opt}}^{v^0} = \mathbf{\Pi}^{v^0} + \frac{\partial \Delta \mathbf{v}^\top}{\partial \mathbf{v}^0} \mathbf{\Pi}^{\Delta v} = \mathbf{\Pi}^{v^0} \quad (85)$$

where

$$\mathbf{\Pi}^{v^0} = \mathbf{\Pi}^{p,v} + \mathbf{\Pi}_p^{s,v} + \mathbf{\Pi}_e^{s,v} + \mathbf{\Pi}_h^{s,v^0}. \quad (86)$$

Fore example, the corresponding second-order derivative $\mathbf{\Pi}_{\text{opt}}^{uu}$ is

$$\mathbf{\Pi}_{\text{opt}}^{uu} = \mathbf{\Pi}^{uu} + \mathbf{\Pi}^{u\Delta v} \frac{\partial \Delta \mathbf{v}}{\partial \mathbf{u}} + \left(\mathbf{\Pi}^{u\Delta v} \frac{\partial \Delta \mathbf{v}}{\partial \mathbf{u}} \right)^\top + \frac{\partial \Delta \mathbf{v}^\top}{\partial \mathbf{u}} \mathbf{\Pi}^{\Delta v \Delta v} \frac{\partial \Delta \mathbf{v}}{\partial \mathbf{u}} + \cancel{\frac{\partial^2 \Delta \mathbf{v}}{\partial \mathbf{u}^2} \mathbf{\Pi}^{\Delta v}} \quad (87)$$

since $\mathbf{\Pi}^u = \mathbf{\Pi}^{\Delta v} = \mathbf{0}$ at an equilibrium configuration. Therefore, neither axial degrees of freedom nor third-order derivatives are required for the optimization. Like previously, remaining state variables \mathbf{u} are eliminated for the optimization by using the gradient matrix \mathbf{G}^{v^0} .

7 Optimization of Example Structures

7.1 Shape Optimization

Two example structures are subsequently used to demonstrate the performance of the proposed algorithm. Both are based on the same reference configuration and optimized for the same target shapes and associated pressure sets (Figure 11). It can be seen that the structure consists of two cell rows with 59 hexagonal and 60 pentagonal cells. The first, second target shape is a half, full circle. The presented results are based on a complete simulation and optimization of the structures. Structural symmetry was not taken into account. Furthermore, optimized cell side lengths vary along the structure due to edge effects so that it is not possible to solve this problem by investigating only a few cells. Hinge eccentricities “ \mathbf{w} ”, rotational springs “ \mathbf{x}_κ ”, axial springs “ \mathbf{x}_h ” and the estimated weighting factors η_{12}/η_{21} after 500 iterations are

| | | first example | second example |
|-----------------------|--------|---------------|----------------|
| " d " | [mm] | 10 | 0 |
| " e " | [N] | 2,083 | 0 |
| " h " | [N/mm] | ∞ | 5,000 |
| η_{12}/η_{21} | [-] | 0.65 | 0.76 |

Note that previous values refer to a cellular structure with a unit depth. Equilibrium shapes, axial cell side stresses and convergence plots for both examples are shown in Figure 12. It can be seen that deviations from the reference configuration are smaller if rotational springs are non-zero. Both examples require only a few iterations for finding their equilibrium configurations. Convergence plots and equilibrium shapes as well as axial cell side stresses are shown in Figure 13. Note that the gradient based approach is used for the first 500 optimization steps. Weighting factors are then estimated and the potential based approach is used to complete the optimizations within a few iterations. Combining the gradient and potential based approach significantly reduces the total number of iterations. It can be seen that the optimized cell side lengths of both structures differ significantly. This is due to the fact that the first structure requires more extreme cell geometries to provide the bending energy for the cell side deformations. This is also highlighted by the η_{12}/η_{21} ratios. Recall that $\eta_{12}/\eta_{21} = 1$ if the potential energy of a cellular structure is identical for both pressure sets.

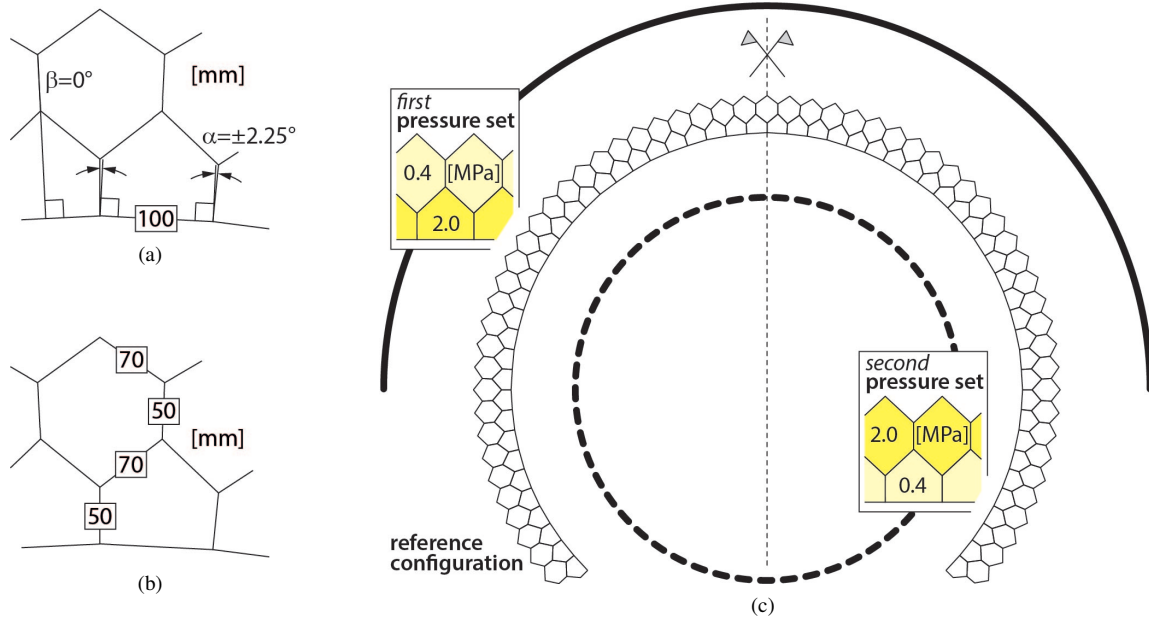
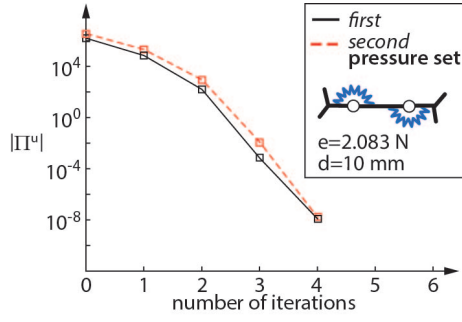


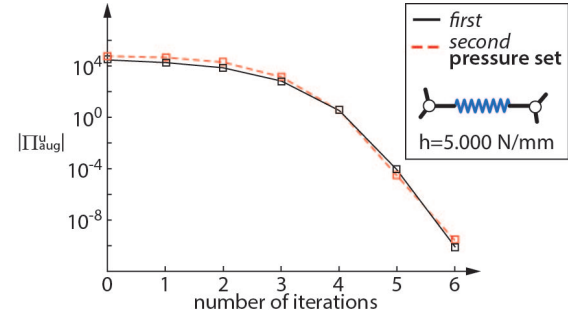
Figure 11: (a) Reference state variables, (b) initial cell side lengths and (c) target shapes with associated pressure sets.

7.2 Contact Optimization

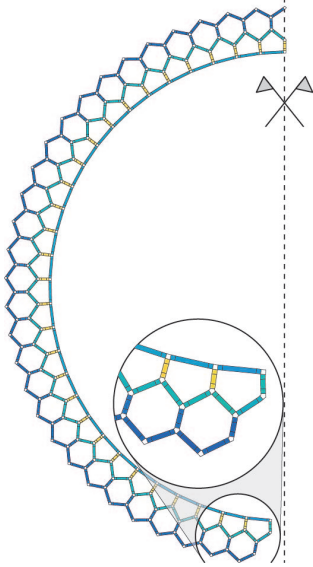
Previous examples demonstrate the optimization of cell side lengths for given target shapes. However, a cellular structure can be optimized for both, target shapes and loads. For example, the optimal geometry of an aircraft's leading, trailing edge is linked to a certain pressure distribution. Hence it is necessary to optimize an adaptive structure such that it possesses the desired geometries for given loads. Another example is the shape optimization for an optimal distribution of contact forces. Figure 14 shows a cantilever with equilibrium configurations that reassemble a straight line and a quarter circle. Note that the second equilibrium configuration penetrates a circular obstacle. Enforcing the contact between structure and obstacle results in a single contact point. In contrast, the optimized structure possesses a contact region that comprises ten cell sides. It can be seen that, although the total contact force is larger, the force at each contact point is only 0.1 N/mm.



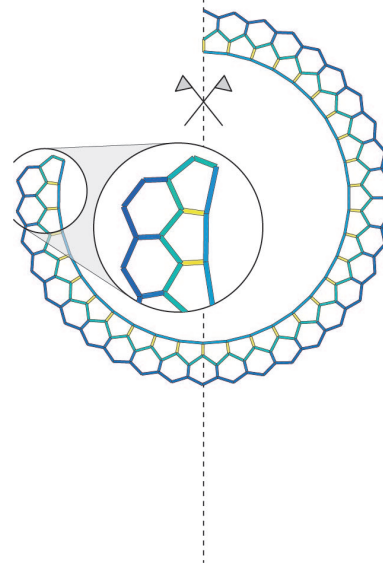
(a)



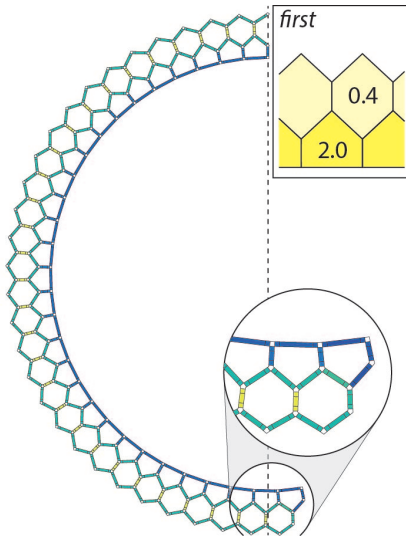
(b)



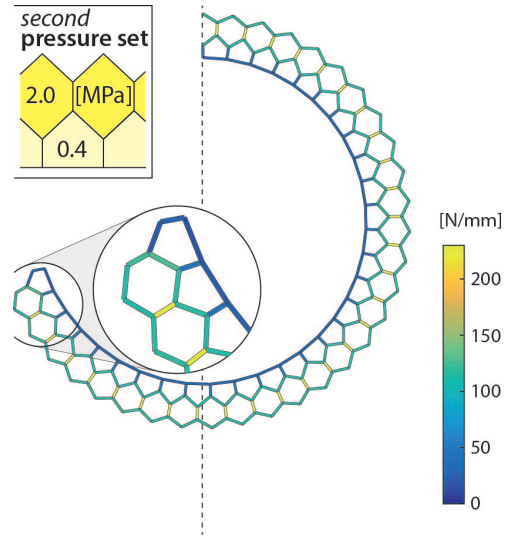
(c)



(d)

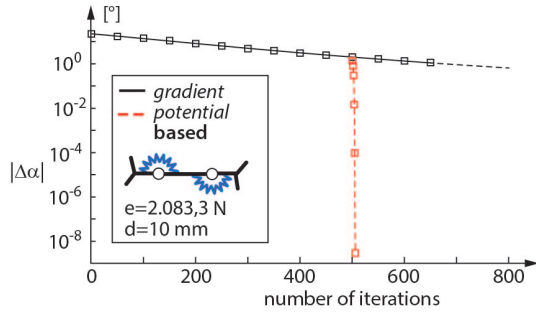


(e)

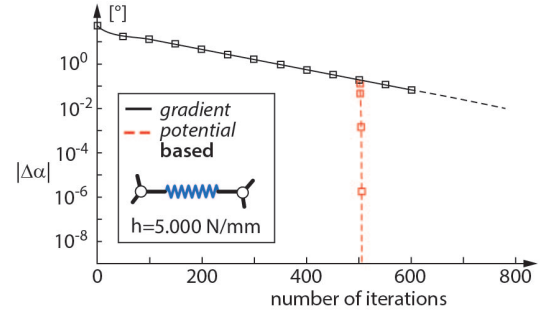


(f)

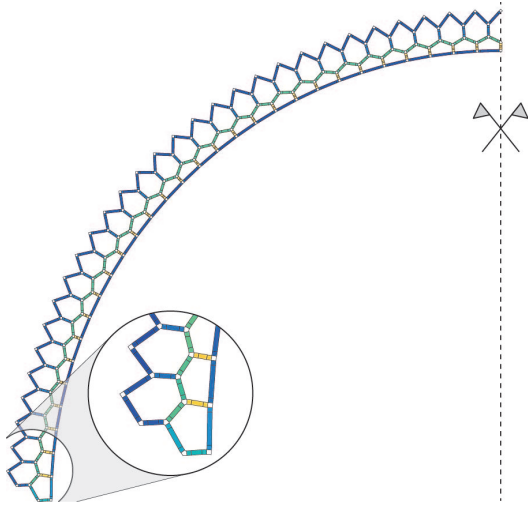
Figure 12: Cellular structure with hinge eccentricities and rotational springs: (a) Convergence and equilibrium shape with axial cell side stresses of (c) first and (e) second pressure set. Cellular structure with axial cell side springs: (b) Convergence and equilibrium shape with axial cell side stresses of (d) first and (f) second pressure set.



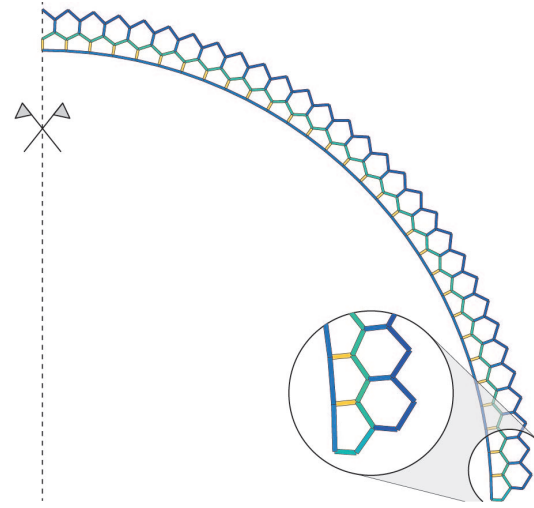
(a)



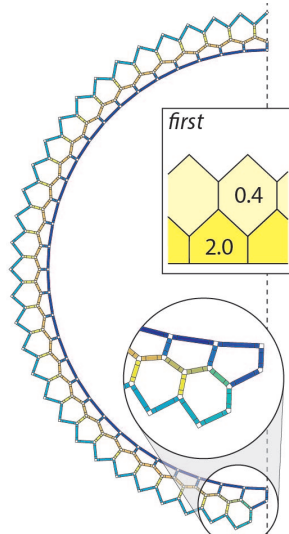
(b)



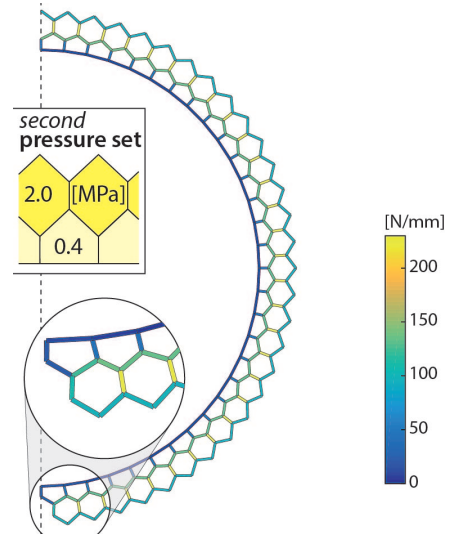
(c)



(d)



(e)



(f)

Figure 13: Cellular structure with hinge eccentricities and rotational springs: (a) Convergence of optimization and equilibrium shape with axial cell side stresses of (c) first and (e) second pressure set. Cellular structure with axial cell side springs: (b) Convergence of optimization and equilibrium shape with axial cell side stresses of (d) first and (f) second pressure set.

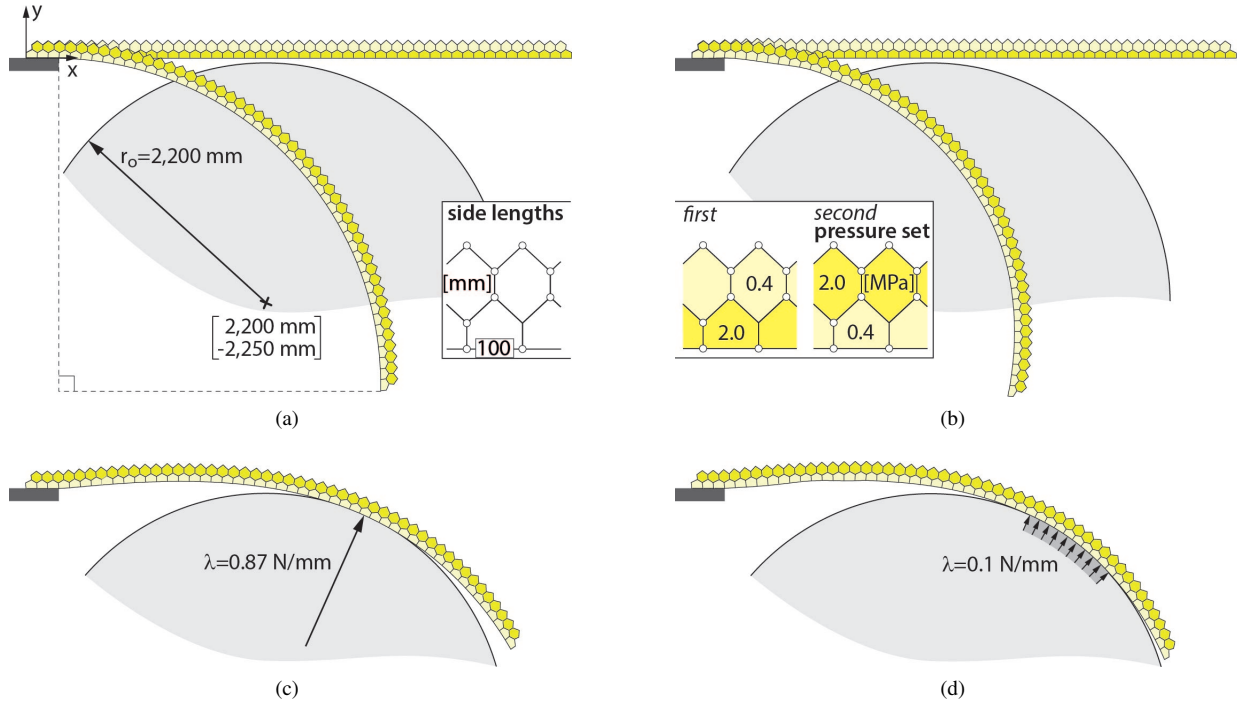


Figure 14: (a) Initial cellular structure with 50 base pentagons deforms into a straight line and a quarter circle (supported base sides are always straight). Circular obstacle is penetrated by second equilibrium shape. (b) Optimized structure with an improved contact force distribution. Contact force of (c) initial and (d) optimized cellular structure.

It is subsequently shown how a cellular structure can be optimized for certain contact forces. The cartesian coordinates of the outer pentagonal nodes can be written as a function of state variables \mathbf{u}_α as

$$\begin{bmatrix} x_i & y_i \end{bmatrix}^\top = \begin{bmatrix} x_{i-1} & y_{i-1} \end{bmatrix}^\top + a_i \begin{bmatrix} \cos\left(\sum_{j=0}^{i-1} \Delta\alpha_j\right) & -\sin\left(\sum_{j=0}^{i-1} \Delta\alpha_j\right) \end{bmatrix}^\top \quad (88)$$

where the assumed boundary conditions are

$$\begin{bmatrix} x_0 & y_0 \end{bmatrix}^\top = \begin{bmatrix} 0 & 0 \end{bmatrix}^\top \quad \text{and} \quad \begin{bmatrix} \alpha_0 & \alpha_1 & \alpha_2 \end{bmatrix}^\top = \begin{bmatrix} 0 & 0 & 0 \end{bmatrix}^\top. \quad (89)$$

A cell side penetrates a circular obstacle with a radius r_o if

$$r(\xi) < r_o \quad \text{for any} \quad \xi \in [0, 1] \quad (90)$$

where $r(\xi)$ is the distance between the obstacle center and the cell side so that

$$r = \sqrt{((x_o - x_i) - (x_{i+1} - x_i)\xi)^2 + ((y_o - y_i) - (y_{i+1} - y_i)\xi)^2} = \sqrt{r_i^2 + 2(r_{i,x}a_{i,x} + r_{i,y}a_{i,y})\xi + a_i^2\xi^2}. \quad (91)$$

Note that $[x_o \ y_o]^\top$ are the cartesian coordinates of the center of the obstacle and $[a_x \ a_y]^\top$ are the vector components of cell side a . The radius $r(\xi)$ of a cell side is minimal for

$$\frac{\partial r^2}{\partial \xi} = 0 \quad \text{so that} \quad \xi_{\min} = -\frac{r_{i,x}a_{i,x} + r_{i,y}a_{i,y}}{a_i^2}. \quad (92)$$

The change of state variables and Lagrange multipliers at an equilibrium configuration with respect to cell side lengths \mathbf{v} is

$$\begin{bmatrix} \frac{\partial \alpha}{\partial \lambda_r} \\ \frac{\partial \mathbf{v}}{\partial \lambda_r} \\ \frac{\partial \mathbf{v}}{\partial \lambda_c} \\ \frac{\partial \mathbf{v}}{\partial \mathbf{v}} \end{bmatrix} = - \begin{bmatrix} \mathbf{\Pi}^{\mathbf{uu}} + \sum_{i=1}^{n^{\lambda_r}} \frac{\partial^2 r_{\min,i}}{\partial \alpha^2} \lambda_r^i & \frac{\partial \mathbf{r}_{\min}}{\partial \alpha}^\top & \frac{\partial \mathbf{c}}{\partial \alpha}^\top \\ \frac{\partial \mathbf{r}_{\min}}{\partial \alpha} & \mathbf{0} & \mathbf{0} \\ \frac{\partial \mathbf{c}}{\partial \alpha} & \mathbf{0} & \mathbf{0} \end{bmatrix}^{-1} \begin{bmatrix} \mathbf{\Pi}^{\mathbf{uv}} \\ \mathbf{0} \\ \mathbf{0} \end{bmatrix} \quad (93)$$

where $r_{\min} = r(\xi_{\min})$ and \mathbf{c} are linear constraints for the boundary conditions. The part of the gradient matrix \mathbf{G} that corresponds to the second pressure set is build from $\partial \lambda_r / \partial \mathbf{v}$. Like in previous examples, the contact force optimization is performed by successively using a gradient and potential based approach. Note that convergence details are not provided since they do not differ substantially from previous examples.

8 Coupling of Numerical and Geometric Model

The numerical framework approximates cellular structures by using eccentric cell corner hinges and rotational, axial springs. This is a necessary simplification for an efficient optimization. However, eccentricities and springs need to be iteratively correlated to the geometry of a cellular structure before it can be build with the desired shape changing properties. The numerical and geometric model of a single cell corner is shown in Figure 15. It is subsequently outlined how both models can be closely coupled. The vector \mathbf{m} that consists of axial forces, cell corner rotations and cell side lengths is known from the numerical model for each pressure set. Axial forces, cell corner rotations are used

since they have to be carried, sustained by cell corners. Their dependence on cell side springs is small. In contrast, axial strains and bending moments depend heavily on cell side springs. The parameters ω of the geometric model can be optimized for \mathbf{m} such that the cross sectional area A of a cell corner is minimized for a given stress constraint $\sigma_{\max} = \sigma_{\text{ult}}$ so that

$$\omega^{i+1} = \omega^i - (\mathbf{A}^{\omega\omega})^{-1} \mathbf{A}^{\omega} \quad (94)$$

where $\mathbf{A}^{\omega\omega}$ is augmented with a Lagrange multiplier so that

$$\frac{\partial \sigma_{\max}}{\partial \omega} (\omega^{i+1} - \omega^i) = \sigma_{\text{ult}} - \sigma_{\max} \quad (95)$$

Note that this constraint considers all pressure sets. The constraint can be replaced at an optimized configuration with

$$\frac{\partial \sigma_{\max}}{\partial \omega} (\omega^{i+1} - \omega^i) = \frac{\partial \sigma_{\max}}{\partial m_j}. \quad (96)$$

to obtain the gradient matrix

$$\mathbf{G}^{\mathbf{m}} = \begin{bmatrix} \frac{\partial \omega_1}{\partial m_1} & \cdots & \frac{\partial \omega_1}{\partial m_{n^m}} \\ \vdots & \ddots & \vdots \\ \frac{\partial \omega_{n^\omega}}{\partial m_1} & \cdots & \frac{\partial \omega_{n^\omega}}{\partial m_{n^m}} \end{bmatrix}. \quad (97)$$

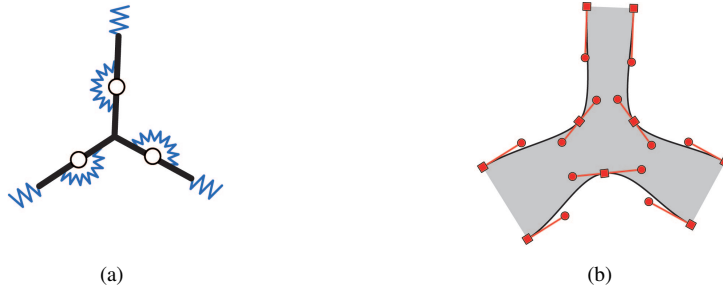


Figure 15: (a) Eccentric cell corner hinges and rotational, axial springs of numerical model. (b) Anchor and control points of geometric model.

The geometric parameters at the interface of neighbouring cell corners are coupled so that C^1 continuity is preserved at any point. Hinge eccentricities \mathbf{w} , rotational \mathbf{x}_Δ and axial \mathbf{x}_κ springs can be obtained from the geometric model. For example, the first-order derivative of \mathbf{w} with respect to \mathbf{m} is

$$\frac{\partial \mathbf{w}}{\partial \mathbf{m}} = \mathbf{G}^{\mathbf{m}\top} \frac{\partial \mathbf{w}}{\partial \omega}. \quad (98)$$

Derivatives of vector \mathbf{m} with respect to state variables \mathbf{u} and cell side lengths \mathbf{v} are known from the numerical model. Hence it is possible to obtain derivatives of, for example, hinge eccentricities \mathbf{w} with respect to state variables \mathbf{u} so that

$$\frac{\partial \mathbf{w}}{\partial \mathbf{u}} = \frac{\partial \mathbf{w}}{\partial \mathbf{m}} \frac{\partial \mathbf{m}}{\partial \mathbf{u}}. \quad (99)$$

These terms can then be used to fully couple the geometric and numerical model.

9 Conclusions

This article presented a computational framework for the simulation and optimization of compliant pressure actuated cellular structures. It complements previous work [11] by taking into account an arbitrary number of cell rows, rotational, axial springs and hinge eccentricities at cell corners. It was shown that the proposed method reduces to the previously published work if hinge eccentricities and rotational, axial springs are negligible. The convergence rate of the optimization was significantly enhanced by combining a gradient and potential based approach. Several examples were presented that demonstrate the quadratic convergence rate for both, the computation of equilibrium configurations and optimal cell side lengths. Finally, it was shown that the parameters of the proposed framework can be tightly coupled to the geometry of a cellular structure. (*An early version of this article [14] was uploaded on arXiv in March 2014.*)

References

- [1] Dittrich, K. (2005), Cellular actuator device and methods of making and using same, *US Patent*, **2005/0029406 A1**.
- [2] Felippa, C.A. and Haugen, B. (2005), A unified formulation of small-strain corotational finite elements: I. Theory, *Computer Methods in Applied Mechanics and Engineering*, **194**, 2285-2335.
- [3] Guiducci, L., Fratzl, P. Brechet, Y.J.M. and Dunlop, J.W.C. (2014), Pressurized honeycombs as soft actuators: a theoretical study, *Journal of the Royal Society Interface*, **6**.
- [4] Guiducci, L., Weaver, J.C., Brechet, Y.J.M., Fratzl, P. and Dunlop J.W.C. (2015), The geometric Design and Fabrication of Actuating Cellular Structures, *Advanced Materials Interfaces*, **2**.
- [5] Huber, J.E., Fleck, N.A., Ashby, M.F. (1997), The selection of mechanical actuators based on performance indices, *Proceedings of the Royal Society A* **453** (2185-2205).
- [6] Sun, J., Gao, H., Scarpa, F., Lira, C., Liu, Y. and Leng, J. (2014), Active inflatable auxetic honeycomb structural concept for morphing wingtips, *Smart Materials and Structures* **23**.
- [7] Kerstens, S., Decraemer, W.F., Verbelen, J.P. (2001), Cell walls at the plant surface behave mechanically like fiber-reinforced composite materials, *Plant Physiology*, **127**.
- [8] Khire, R., Dessel, S., Messac, A. and Mullur, A. (2006), Study of a honeycomb-type rigidified inflatable structure for housing. *Journal of Structural Engineering*, **132**, 1664-1672.
- [9] Lv, J., Zhang, H.W. and Yang, D.S. (2013), Multiscale method for mechanical analysis of heterogeneous materials with polygonal microstructures, *Mechanics of Materials*, **56**.
- [10] Lv, J., Liu, H. and Zhang, H.W. (2014), A multiscale co-rotational method for geometrically nonlinear shape morphing of 2D fluid actuated cellular structures, **79**.
- [11] Pagitz, M., Lamacchia, E. and Hol, J.M.A.M. (2012), Pressure-actuated cellular structures, *Bioinspiration&Biomimetics*, **7**.
- [12] Pagitz, M. and Hol, J.M.A.M. (2012), A morphing structure and method for morphing a structure, *Patent NL 2006936*.
- [13] Pagitz, M., Pagitz, M.H. and Hühne, C. (2014), A Modular Approach to Adaptive Structures, *Bioinspiration&Biomimetics*, **9(4)**.
- [14] Pagitz, M. (2014), Compliant Pressure Actuated Cellular Structures, *arXiv 1403.2197*.
- [15] Pagitz, M. and Kappel, E. (2014), Design of Pressure Actuated Cellular Structures, *arXiv 1403.4033*.
- [16] Stahlberg, R., Taya, M. (2006), Biomimetics - Biologically inspired technologies, *CRC Press*, **Chapter 19**.
- [17] Luo, Q., Tong, L. (2013), Adaptive pressure-controlled cellular structures for shape morphing I: design and analysis, *Smart Materials and Structures*, **22**.
- [18] Vos, R., Barret, R.M., Romkes, R. (2010), Mechanics of pressure-adaptive honeycomb, *Journal of Intelligent Material Systems and Structures*, **22**.
- [19] Wereley, N.M., Sater, J.M. (2012), Plants and Mechanical Motion, *DEStech Publications*.